PHYSICAL REVIEW D **88,** 014031 (2013)

Charmless $B_{u,d,s} \to VT$ decays in perturbative QCD approach

C. S. Kim,[1,*] Run-Hui Li,[1] Freddy Simanjuntak,[1] and Z. T. Zou[2]

[1]*Department of Physics and IPAP, Yonsei University, Seoul 120-479, Korea*

[2]*Institute of High Energy Physics, P.O. Box 918(4), Beijing 100049, China*

(Received 30 April 2013; published 22 July 2013)

Motivated by the experimental data, we study charmless $B_{u,d,s} \to VT$ (V and T denote light vector and tensor mesons, respectively) decays in the perturbative QCD approach. The predictions of branching ratios, polarization fractions, and direct CP violations are given in detail. Specifically, within this approach we have calculated the polarization fractions and the branching ratios of $B \to \phi(K_2^{*-}, \bar{K}_2^{*0})$ which agree well with the observed experimental data; however, the branching ratios of $B \to \omega(K_2^{*-}, \bar{K}_2^{*0})$ are hard to be explained, where the polarization fractions are well accommodated. The tree dominated channels with a vector meson emitted have a longitudinal polarization fraction of 90%, while the penguin dominating ones have subtle polarization fractions. Fortunately, most branching ratios of $B_{u,d}$ decays are of the order 10^{-6}, which would be straightforward for experimental observations. For the B_s decays the branching ratios can reach the order of 10^{-6} in tree dominated decays, while in penguin dominated decays those are of the order of 10^{-7} which require more experimental data to be observed.

DOI: 10.1103/PhysRevD.88.014031 PACS numbers: 13.25.Hw, 12.15.Hh

I. INTRODUCTION

Flavor physics has been thoroughly investigated for many years with the advent of B factories. As more and more experimental data is accumulated, flavor physics plays an important role in the precision test of the standard model (SM) and beyond the SM as well as studying the properties of many light hadrons. A few $B \to VT$ decay channels have been already reported by the *BABAR* Collaboration [1–3], which makes the B to tensor meson[1] decays gain more and more attention.

Even before the experimental reports there had been already a couple of works [4,5], which studied the $B \to VT$ decays involving a charmed tensor meson under the quark model. Here we would like to consider the charmless $B \to VT$ decays instead. As early works, these charmless decays had been also studied in the framework of generalized factorization [6] and in the Isgur-Scora-Grinstein-Wise updated model [7,8]. Later these decays were again studied in the covariant light-front approach in Ref. [9]. Polarizations of $B \to VT$ decays as well are studied in Ref. [10]. However, most of the branching ratios in the early works are not predicted precisely, which are usually one or two order smaller than the experimental data. This may indicate that some contributions, such as the nonfactorizable and annihilation contributions, are very important in these decays, which are not included in those early works. It has become very urgent to investigate these contributions by employing proper theoretical models. In Ref. [11] the authors accommodated the experimental data with the QCD factorization (QCDF) approach [12], which deals with these additional contributions in a very subtle and technical way. Here we want to adopt yet another theoretical approach, the perturbative QCD (pQCD) approach [13], which calculates the nonfactorizable and annihilation contributions in a theoretically systematical way. These investigations will offer us more detailed knowledge about the dynamics of $B \to VT$ decays, which is one reason why those decays are worthy to be studied again.

Another reason why $B \to VT$ decays are meaningful is the interesting polarization phenomena. In $B \to VV$ decays, the transversely polarized contributions of some penguin dominating channels, such as $B \to (\phi, \rho)K^*$, are nearly the same as the longitudinal ones [14]. This is quite different from the prediction of the naive factorization, in which the longitudinal polarization always dominates. However, in $B \to VT$ decays, such as $B \to \phi K_2^*$, the experimental data indicate that the longitudinal polarization is much larger, while for $B \to \omega K_2^*$ the longitudinal polarization takes only about a half contribution. Earlier models such as naive factorization cannot give us any satisfied explanation. Therefore, employing theoretically more complete models, such as the QCDF, the pQCD, and the soft collinear effective theory, to understand the phenomena becomes very important.

In a recent paper [15], the authors studied the light cone distribution amplitudes of the tensor mesons, which make the calculation of $B \to VT$ decays possible for the QCDF and the pQCD approach. In their following paper [11], by extracting inputs from the experimental data they accommodated $B \to VT$ decays in the frame of the QCDF. However, some subtle dynamical phenomena are not yet fully understood, which inspires us to explore these decays under another approach. The pQCD approach based on the k_T factorization has already been used to explore many two body exclusive decays of B meson. The form factors of B to a tensor meson transition have already been calculated under this approach

*Corresponding author.
cskim@yonsei.ac.kr

[1]Tensor mesons with $J^P = 2^+$ have recently become one of many hot topics.

[16]. There are already a few investigations on the B to a pseudoscalar and a tensor [17] as well as a charmed meson and a tensor meson decay [18–20]. The predictions based on the pQCD can accommodate many experimental data well, for example, see Ref. [21]. Therefore in this work we will adopt this approach to our analysis.

The paper is organized as follows. In Sec. II, all the details of the theoretical frameworks are listed, including the notation conventions, the Hamiltonian, the kinematics definitions, the wave functions which are used as the inputs in the pQCD approach, and the analytic formulas for the Feynman diagrams in the pQCD approach. The numerical results and discussions are given in Sec. III, and the last section is for the summary. In the Appendix we collect the expressions of common pQCD functions.

II. THEORETICAL DETAILS

A. Hamiltonian and kinematics

We start from the common low energy effective Hamiltonian used in B physics calculations, which are given [22] as

$$\mathcal{H}_{\rm eff} = \frac{G_F}{\sqrt{2}}\Big\{\sum_{q=u,c} V_{qb}V_{qD}^*[C_1(\mu)O_1^q(\mu) + C_2(\mu)O_2^q(\mu)] - V_{tb}V_{tD}^*\Big[\sum_{i=3}^{10} C_i(\mu)O_i(\mu)\Big]\Big\} + \text{H.c.}, \tag{1}$$

where $D = s, d$ stands for a down-type light quark, $V_{qb(D)}$ and $V_{tb(D)}$ are Cabibbo-Kobayashi-Maskawa (CKM) matrix elements. Functions O_i $(i = 1, \ldots, 10)$ are local four-quark operators or the moment-type operators:

(i) current-current (tree) operators

$$O_1^q = (\bar{q}_\alpha b_\beta)_{V-A}(\bar{D}_\beta q_\alpha)_{V-A}, \qquad O_2^q = (\bar{q}_\alpha b_\alpha)_{V-A}(\bar{D}_\beta q_\beta)_{V-A}, \tag{2}$$

(ii) QCD penguin operators

$$O_3 = (\bar{D}_\alpha b_\alpha)_{V-A}\sum_{q'}(\bar{q}'_\beta q'_\beta)_{V-A}, \qquad O_4 = (\bar{D}_\beta b_\alpha)_{V-A}\sum_{q'}(\bar{q}'_\alpha q'_\beta)_{V-A}, \tag{3}$$

$$O_5 = (\bar{D}_\alpha b_\alpha)_{V-A}\sum_{q'}(\bar{q}'_\beta q'_\beta)_{V+A}, \qquad O_6 = (\bar{D}_\beta b_\alpha)_{V-A}\sum_{q'}(\bar{q}'_\alpha q'_\beta)_{V+A}, \tag{4}$$

(iii) electroweak penguin operators

$$O_7 = \frac{3}{2}(\bar{D}_\alpha b_\alpha)_{V-A}\sum_{q'} e_{q'}(\bar{q}'_\beta q'_\beta)_{V+A}, \qquad O_8 = \frac{3}{2}(\bar{D}_\beta b_\alpha)_{V-A}\sum_{q'} e_{q'}(\bar{q}'_\alpha q'_\beta)_{V+A}, \tag{5}$$

$$O_9 = \frac{3}{2}(\bar{D}_\alpha b_\alpha)_{V-A}\sum_{q'} e_{q'}(\bar{q}'_\beta q'_\beta)_{V-A}, \qquad O_{10} = \frac{3}{2}(\bar{D}_\beta b_\alpha)_{V-A}\sum_{q'} e_{q'}(\bar{q}'_\alpha q'_\beta)_{V-A}, \tag{6}$$

where α and β are color indices and q' are the active quarks at the scale m_b, i.e., $q' = (u, d, s, c, b)$. At the tree level, the operators $O_{7\gamma}$ and O_{8g} do not contribute, thus they are not listed here. The left-handed current is defined as $(\bar{q}'_\alpha q'_\beta)_{V-A} = \bar{q}'_\alpha\gamma_\nu(1-\gamma_5)q'_\beta$ and the right-handed current $(\bar{q}'_\alpha q'_\beta)_{V+A} = \bar{q}'_\alpha\gamma_\nu(1+\gamma_5)q'_\beta$. The projection operators are defined as $P_L = (1-\gamma_5)/2$ and $P_R = (1+\gamma_5)/2$. The combinations a_i of Wilson coefficients are defined as usual [23]:

$$\begin{aligned} a_1 &= C_2 + C_1/3, & a_2 &= C_1 + C_2/3,\\ a_3 &= C_3 + C_4/3, & a_4 &= C_4 + C_3/3,\\ a_5 &= C_5 + C_6/3, & a_6 &= C_6 + C_5/3,\\ a_7 &= C_7 + C_8/3, & a_8 &= C_8 + C_7/3,\\ a_9 &= C_9 + C_{10}/3, & a_{10} &= C_{10} + C_9/3. \end{aligned} \tag{7}$$

The calculation is carried out in the rest frame of B meson, the momenta of B meson (p_B), tensor meson (p_2) and vector meson (p_3) are defined in the light cone coordinates as

$$p_B = \frac{m_B}{\sqrt{2}}(1, 1, \mathbf{0_T}), \qquad p_2 = \frac{m_B}{\sqrt{2}}(1, r_2^2, \mathbf{0_T}), \qquad p_3 = \frac{m_B}{\sqrt{2}}(r_3^2, 1, \mathbf{0_T}) \tag{8}$$

with $r_2 = m_T/m_B$ and $r_3 = m_V/m_B$. In the calculation of the pQCD, the momenta of the quarks are also related, and they are defined as follows:

$$k_1 = \Big(0, x_1\frac{m_B}{\sqrt{2}}, \mathbf{k_{1T}}\Big), \qquad k_2 = \Big(x_2\frac{m_B}{\sqrt{2}}, 0, \mathbf{k_{2T}}\Big), \qquad k_3 = \Big(0, x_3\frac{m_B}{\sqrt{2}}, \mathbf{k_{3T}}\Big), \tag{9}$$

where $k_{1,2,3}$ are the momenta of the light antiquark in B meson, quarks in tensor and vector mesons, respectively.

B. Wave functions

1. B meson

The $B_{(s)}$ meson wave functions are decomposed into the following Lorentz structures:

$$\int \frac{d^4z}{(2\pi)^4} e^{ik_1\cdot z}\langle 0|\bar{b}_\alpha(0)d_\beta(z)|B_{(s)}(P_1)\rangle = \frac{i}{\sqrt{2N_c}}\left\{(\not{P}_1 + m_{B_{(s)}})\gamma_5\left[\phi_{B_{(s)}}(k_1) + \frac{\not{n}}{\sqrt{2}}\bar{\phi}_{B_{(s)}}(k_1)\right]\right\}_{\beta\alpha}, \tag{10}$$

where $\phi_{B_{(s)}}(k_1)$ and $\bar{\phi}_{B_{(s)}}(k_1)$ are the leading twist distribution amplitudes. After neglecting the numerically subleading contribution term $\bar{\phi}_{B_{(s)}}(k_1)$ [24], the expression for $\Phi_{B_{(s)}}$ in the momentum space becomes

$$\Phi_{B_{(s)}} = \frac{i}{\sqrt{2N_c}}(\not{P}_1 + m_{B_{(s)}})\gamma_5\phi_{B_{(s)}}(k_1). \tag{11}$$

The calculation of the pQCD is always carried out in the b space, in which we adopt the following model function:

$$\phi_{B_{(s)}}(x,b) = N_{B_{(s)}}x^2(1-x)^2\exp\left[-\frac{1}{2}\left(\frac{xm_{B_{(s)}}}{\omega_b}\right)^2 - \frac{\omega_b^2 b^2}{2}\right], \tag{12}$$

where b is the conjugate space coordinate of $\mathbf{k}_{1T}$. $N_{B_{(s)}}$ is the normalization constant, which is determined by the normalization condition

$$\int_0^1 dx\phi_{B_{(s)}}(x, b=0) = \frac{f_{B_{(s)}}}{2\sqrt{2N_c}}. \tag{13}$$

For $B^\pm$ and B_d^0 decays, we adopt the value $\omega_b = 0.40$ GeV [25], which is supported by intensive pQCD studies [26]. For the B_s meson, we will follow the authors in Ref. [27] and adopt the value $\omega_{b_s} = (0.50 \pm 0.05)$ GeV.

2. Vector meson

The decay constants of the vector mesons are defined by

$$\begin{aligned}\langle 0|\bar{q}_1\gamma_\mu q_2|V(p_3,\epsilon)\rangle &= f_V m_V \epsilon_\mu,\\ \langle 0|\bar{q}_1\sigma_{\mu\nu}q_2|V(p_3,\epsilon)\rangle &= if_V^T(\epsilon_\mu P_{3\nu} - \epsilon_\nu P_{3\mu}).\end{aligned} \tag{14}$$

The longitudinal decay constants of the charged mesons can be extracted experimentally from τ^- decays and those of the neutral ones can be extracted from their e^+e^- decays [28], whereas the transverse decay constants can be calculated by the QCD sum rules [29]. All the constants for the vector mesons in this paper are collected in Table I.

Up to twist-3 the distribution amplitudes of the light vector mesons are summarized as

$$\begin{aligned}\langle V(p_3,\epsilon_L^*)|q_{1\alpha}(0)\bar{q}_{2\beta}(z)|0\rangle &= -\frac{1}{\sqrt{2N_C}}\int_0^1 dx e^{ixp_3\cdot z}[m_V \not{\epsilon}_L^* \phi_V(x) + \not{\epsilon}_L^* \not{p}_3\phi_V^t(x) + m_V\phi_V^s(x)]_{\alpha\beta},\\ \langle V(p_3,\epsilon_T^*)|q_{1\alpha}(0)\bar{q}_{2\beta}(z)|0\rangle &= -\frac{1}{\sqrt{2N_C}}\int_0^1 dx e^{ixp_3\cdot z}[m_V \not{\epsilon}_L^* \phi_V^v(x) + \not{\epsilon}_L^* \not{p}_3\phi_V^T(x) + m_V i\epsilon_{\mu\nu\rho\sigma}\gamma_5\gamma^\mu\epsilon_T^{*\nu}n^\rho v^\sigma\phi_V^a(x)]_{\alpha\beta},\end{aligned} \tag{15}$$

where x is the momentum fraction of the q_2 quark. Here n is the light cone direction along which the meson moves and v is the opposite direction. With $t = 2x - 1$ the expression for the twist-2 distribution amplitudes are given by

$$\begin{aligned}\phi_V(x) &= \frac{3f_V}{\sqrt{2N_C}}x(1-x)[1 + a_1^\parallel C_1^{3/2}(t) + a_2^\parallel C_2^{3/2}(t)],\\ \phi_V^T(x) &= \frac{3f_V}{\sqrt{2N_C}}x(1-x)[1 + a_1^\perp C_1^{3/2}(t) + a_2^\perp C_2^{3/2}(t)],\end{aligned} \tag{16}$$

and the corresponding values of the Gegenbauer moments are [30]

$$\begin{aligned} &a_{2\rho}^\parallel = a_{2\omega}^\parallel = 0.15 \pm 0.07, \quad a_{1K^*}^\parallel = 0.03 \pm 0.02,\\ &a_{2K^*}^\parallel = 0.11 \pm 0.09, \quad a_{2\phi}^\parallel = 0.18 \pm 0.08,\\ &a_{2\rho}^\perp = a_{2\omega}^\perp = 0.14 \pm 0.06, \quad a_{1K^*}^\perp = 0.04 \pm 0.03,\\ &a_{2K^*}^\perp = 0.10 \pm 0.08, \quad a_{2\phi}^\perp = 0.14 \pm 0.07.\end{aligned} \tag{17}$$

We adopt the asymptotic form for the twist-3 distribution amplitudes:

$$\begin{aligned}\phi_V^t(x) &= \frac{3f_V^T}{2\sqrt{6}}t^2, \quad \phi_V^s(x) = \frac{3f_V^T}{2\sqrt{6}}(-t),\\ \phi_V^v(x) &= \frac{3f_V}{8\sqrt{6}}(1+t^2), \quad \phi_V^a(x) = \frac{3f_V}{4\sqrt{6}}(-t).\end{aligned} \tag{18}$$

3. Tensor meson

In the quark model, the tensor meson with $J^{PC} = 2^{++}$ has the angular momentum $L = 1$ and spin $S = 1$. The ground $SU(3)$ nonet states consist of $a_2(1320)$, $f_2(1270)$, $f_2'(1525)$, and $K_2^*(1430)$. Mixing exists for the $f_2(1270)$ and $f_2'(1525)$, just as the η and η' mixing, and their wave functions can be expressed as

$$\begin{aligned} f_2 &= f^q\cos\theta_{f_2} + f^s\sin\theta_{f_2},\\ f_2' &= f^q\cos\theta_{f_2} - f^s\sin\theta_{f_2},\end{aligned} \tag{19}$$

TABLE I. The decay constants of vector mesons (in MeV).

f_ρ	f_{K^*}	f_ω	f_ϕ	f_ρ^T	$f_{K^*}^T$	f_ω^T	f_ϕ^T
209 ± 2	217 ± 5	195 ± 3	231 ± 4	165 ± 9	185 ± 10	151 ± 9	186 ± 9

where $f^q = \frac{1}{\sqrt{2}}(u\bar{u} + d\bar{d})$ and $f^s = s\bar{s}$. The mixing angle θ_{f_2} is found to be very small, $\theta_{f_2} = 7.8°$ [14] and $\theta_{f_2} = (9 \pm 1)°$ [31]. Therefore, f_2 is nearly an f^q state and f_2' is mainly f^s.

The spin-2 polarization tensor, which is symmetric and traceless, satisfies $\epsilon^{\mu\nu} p_{2\nu} = 0$ and can be constructed by spin-1 polarization vectors ϵ by

$$\begin{aligned}
\epsilon_{\mu\nu}(\pm 2) &= \epsilon_\mu(\pm)\epsilon_\nu(\pm), \\
\epsilon_{\mu\nu}(\pm 1) &= \frac{1}{\sqrt{2}}[\epsilon_\mu(\pm)\epsilon_\nu(0) + \epsilon_\nu(\pm)\epsilon_\mu(0)], \\
\epsilon_{\mu\nu}(0) &= \frac{1}{\sqrt{6}}[\epsilon_\mu(+)\epsilon_\nu(-) + \epsilon_\nu(+)\epsilon_\mu(-)] \\
&\quad + \sqrt{\frac{2}{3}}\epsilon_\mu(0)\epsilon_\nu(0).
\end{aligned} \tag{20}$$

In the case that the tensor meson is moving along the z axis, the polarizations ϵ can be defined as

$$\epsilon(0) = (|p_2|, 0, 0, E_2)/m_T, \qquad \epsilon(\pm 1) = (0, \mp 1, i, 0)/\sqrt{2}, \tag{21}$$

with E_2 as the energy of the tensor meson. Associating with the tensor momentum defined in Eq. (8), the polarization vectors are given in the light cone coordinates by

$$\begin{aligned}
\epsilon(0) &= (1, -r_2^2, \mathbf{0_T})/(\sqrt{2}r_2), \\
\epsilon(\pm 1) &= (0, 0, \mp 1, i, 0)/\sqrt{2}.
\end{aligned} \tag{22}$$

The decay constants of the tensor mesons are defined as

$$\begin{aligned}
\langle T(p_2)|j_{\mu\nu}(0)|0\rangle &= f_T m_T^2 \epsilon^*_{\mu\nu}, \\
\langle T(p_2)|j_{\mu\nu\rho}(0)|0\rangle &= -if_T^T m_T(\epsilon^*_{\mu\delta} p_{2\nu} - \epsilon^*_{\nu\delta} p_{2\mu}),
\end{aligned} \tag{23}$$

where the currents are defined as

$$\begin{aligned}
j_{\mu\nu}(0) &= \frac{1}{2}[\bar{q}_1(0)\gamma_\mu i\overleftrightarrow{D}_\nu q_2(0) + \bar{q}_1(0)\gamma_\nu i\overleftrightarrow{D}_\mu q_2(0)], \\
j^\dagger_{\mu\nu\rho}(0) &= \bar{q}_2(0)\sigma_{\mu\nu} i\overleftrightarrow{D}_\rho q_1(0)
\end{aligned} \tag{24}$$

with $\overleftrightarrow{D}_\mu = \overrightarrow{D}_\mu - \overleftarrow{D}_\mu$, $\overrightarrow{D}_\mu = \overrightarrow{\partial}_\mu + ig_s A^a_\mu \lambda^a/2$ and $\overleftarrow{D}_\mu = \overleftarrow{\partial}_\mu - ig_s A^a_\mu \lambda^a/2$, respectively. These decay constants have already been studied [32–34] and we use the recently updated ones with the QCD sum rules [15], which are summarized in Table II.

The light cone distribution amplitudes (LCDAs) of the tensor mesons are also recently studied by Ref. [15] and we follow the notations in Ref. [16] to summarize them up to twist-3 as

$$\begin{aligned}
&\langle T(p_2, \epsilon)|q_{1\alpha}(0)\bar{q}_{2\beta}(z)|0\rangle \\
&= \frac{1}{\sqrt{2N_c}}\int_0^1 dx e^{ixp_2\cdot z}\Big[m_T \not{\epsilon}^*_{\bullet L}\phi_T(x) \\
&\quad + \not{\epsilon}^*_{\bullet L}\not{p}_2\phi_T^t(x) + m_T^2\frac{\epsilon_\bullet\cdot v}{p_2\cdot v}\phi_T^s(x)\Big]_{\alpha\beta},
\end{aligned} \tag{25}$$

$$\begin{aligned}
&\langle T(p_2, \epsilon)|q_{1\alpha}(0)\bar{q}_{2\beta}(z)|0\rangle \\
&= \frac{1}{\sqrt{2N_c}}\int_0^1 dx e^{ixp_2\cdot z}[m_T \not{\epsilon}^*_{\bullet T}\phi_T^v(x) + \not{\epsilon}^*_{\bullet T}\not{p}_2\phi_T^T(x) \\
&\quad + m_T i\epsilon_{\mu\nu\rho\sigma}\gamma_5\gamma^\mu \epsilon^{*\nu}_{\bullet T} n^\rho v^\sigma \phi_T^a(x)]_{\alpha\beta},
\end{aligned} \tag{26}$$

with $\epsilon^{0123} = 1$ adopted. Equation (25) is for the longitudinal polarized mesons ($h = 0$) and Eq. (26) for the transverse polarized ones ($h = \pm 1$). x is the momentum fraction associated with the q_2 quark. n is the light cone direction along which the tensor meson moves and v is the opposite direction. $\epsilon_\bullet$ is defined by

$$\epsilon_{\bullet\mu} \equiv \frac{\epsilon_{\mu\nu} v^\nu}{p_2\cdot v} m_T. \tag{27}$$

With the momenta and polarizations defined in the above paragraphs, Eq. (27) can be reexpressed by

$$\epsilon_{\bullet\mu} = \frac{2m_T}{m_B^2}\epsilon_{\mu\nu} p_B^\nu \tag{28}$$

up to the leading power of r_2. We follow the symbols in Ref. [16], and list the expressions of LCDAs as

$$\begin{aligned}
\phi_T(x) &= \frac{f_T}{2\sqrt{2N_c}}\phi_\parallel(x), & \phi_T^t(x) &= \frac{f_T^T}{2\sqrt{2N_c}}h_\parallel^{(t)}(x), \\
\phi_T^s(x) &= \frac{f_T^T}{4\sqrt{2N_c}}\frac{d}{dx}h_\parallel^{(s)}(x), & \phi_T^T(x) &= \frac{f_T^T}{2\sqrt{2N_c}}\phi_\perp(x), \\
\phi_T^v(x) &= \frac{f_T}{2\sqrt{2N_c}}g_\perp^{(v)}(x), & \phi_T^a(x) &= \frac{f_T}{8\sqrt{2N_c}}\frac{d}{dx}g_\perp^{(a)}(x).
\end{aligned} \tag{29}$$

The twist-2 LCDAs can be expanded in terms of the Gegenbauer polynomials with the form

$$\phi_{\parallel,\perp}(x) = 6x(1-x)\sum_{l=1}^{\infty} a_l^{\parallel,\perp} C_l^{3/2}(2x-1), \tag{30}$$

where $a_l^{\parallel,\perp}$ are the coefficients. Since there are no results for the high order Gegenbauer coefficients and the

TABLE II. Decay constants (in unit of MeV) of tensor mesons from Ref. [15].

f_{a_2}	$f^T_{a_2}$	$f_{K_2^*}$	$f^T_{K_2^*}$	$f_{f_2(1270)}$	$f^T_{f_2(1270)}$	$f_{f_2'(1525)}$	$f^T_{f_2'(1525)}$
107 ± 6	105 ± 21	118 ± 5	77 ± 14	102 ± 6	117 ± 25	126 ± 4	65 ± 12

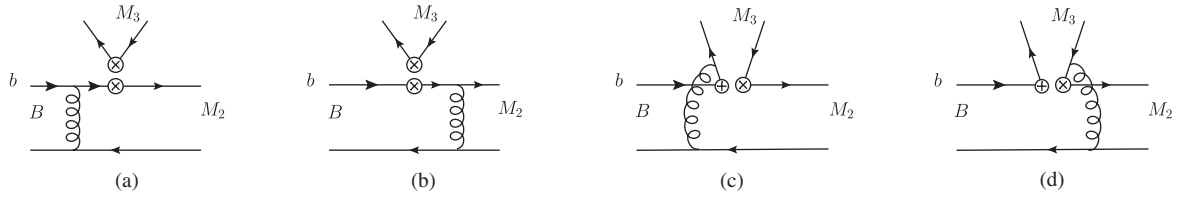

FIG. 1. The emission diagrams with a tensor meson emitted. Diagrams (a) and (b) are the factorizable contributions; diagrams (c) and (d) are nonfactorizable diagrams.

contributions of these high order polynomials are expected to be very small, we adopt the asymptotic form in the calculation, which is given by

$$\phi_{\parallel,\perp}(x) = 30x(1-x)(2x-1) \tag{31}$$

with the normalization conditions

$$\int_0^1 dx(2x-1)\phi_{\parallel,\perp}(x) = 1. \tag{32}$$

By using the QCD equations of motion, the twist-3 two partons distribution amplitudes (DAs) can be related to the twist-2 ones and the tree parton DAs [35,36]. Their expressions for the asymptotic forms are given by [15]

$$\begin{aligned} h_{\parallel}^{(t)}(x) &= \frac{15}{2}(2x-1)(1-6x+6x^2), \\ h_{\parallel}^{(s)}(x) &= 15x(1-x)(2x-1), \end{aligned} \tag{33}$$

$$g_{\perp}^{(a)}(x) = 20x(1-x)(2x-1), \qquad g_{\perp}^{(v)}(x) = 5(2x-1)^3. \tag{34}$$

C. Analytic formulas

In this subsection, we list the pQCD formulas for all the possible Feynman diagrams. In the diagrams we use $M_{2,3}$ to denote the tensor and vector mesons, respectively. At the tree level, the Feynman diagrams in the pQCD can be divided into two types according to their typological structures: the emission diagrams, in which the light quark in the B meson enters one of the light mesons as a spectator, and the annihilation diagrams, in which both of the two quarks in B mesons are absorbed by the electroweak operator. According to the polarizations, we can list the formulas in two parts, the longitudinal polarizations and the transverse ones. For simplicity we only list the amplitude functions for the longitudinal ones. The transverse polarized ones can be calculated in the same way with the corresponding wave functions. The factorizable emission diagrams are shown as the first two diagrams in Fig. 1. Since the tensor meson cannot be generated from the vector or axial vector current, only the vector meson can be emitted. The expressions for all possible Lorentz structures are given as follows.

(i) $(V-A)\,(V-A)$ factorizable emission diagrams:

$$\begin{aligned} F_{\rm vef}^{LL}(a_i) = 8\sqrt{\frac{2}{3}}\pi m_B^4 f_V C_F \int_0^1 dx_1 dx_2 \int_0^{1/\Lambda_{\rm QCD}} b_1 db_1 b_2 db_2 \phi_B(x_1)\Big\{&(r_2(2x_2-1)(\phi_T^t(x_2)-\phi_T^s(x_2)) \\ &+ (2-x_2)\phi_T(x_2))a_i(t_{\rm vef}^1)E_e(t_{\rm vef}^1)h_e\Big(\sqrt{|\alpha_{ef1}^2|},\sqrt{|\beta_{ef1}^2|},b_2,b_1\Big)S_t(x_2) \\ &- 2r_2\phi_T^s(x_2)a_i(t_{\rm vef}^2)E_e(t_{\rm vef}^2)h_e\Big(\sqrt{|\alpha_{ef2}^2|},\sqrt{|\beta_{ef2}^2|},b_1,b_2\Big)S_t(x_1)\Big\}, \end{aligned} \tag{35}$$

where the explicit expressions of scales $t_{\rm vef}^{1,2}$, the production of coupling α_s and Sudakov factor $E_e(t_{\rm vef}^{1,2})$, the function of hard kernel h_e, the parameters $\alpha_{(ef1,ef2)}^2$ and $\beta_{(ef1,ef2)}^2$, and the jet function $S_t(x)$ are all collected in the Appendix. In the following analytic formulas, the expressions of all the additional functions can also be found in the same Appendix.

(ii) $(V-A)\,(V+A)$ factorizable emission diagrams:

$$F_{\rm vef}^{LR}(a_i) = F_{\rm vef}^{LL}(a_i), \tag{36}$$

(iii) $(S-P)\,(S+P)$ factorizable emission diagrams:

$$F_{\rm vef}^{SP}(a_i) = 0. \tag{37}$$

There are two possible types of nonfactorizable emission diagrams, one has the vector meson emitted and the other has the tensor meson emitted. They are depicted by the last two diagrams of Figs. 1 and 2, respectively. We use the index ten to represent the tensor meson emission and ven for vector meson emission. The expressions are given by

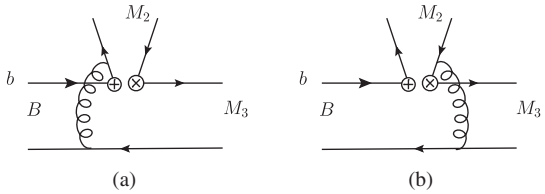

FIG. 2. The nonfactorizable emission diagrams with a tensor meson emitted.

(i) $(V-A)\,(V-A)$ nonfactorizable emission diagrams with vector meson emission:

$$F_{\rm ven}^{LL}(a_i) = \frac{32}{3}\pi m_B^4 C_F \int_0^1 dx_1 dx_2 dx_3 \int_0^{1/\Lambda_{\rm QCD}} b_1 db_1 b_3 db_3 \phi_B(x_1)\phi_V(x_3)\Big\{(r_2(1-x_2)(\phi_T^s(x_2)+\phi_T^t(x_2)) + x_3\phi_T(x_2))a_i(t_{\rm ven}^1)E_{\rm en}(t_{\rm ven}^1,1,2)h_{\rm en}\Big(\sqrt{|\alpha_{\rm en1}^2|},\sqrt{|\beta_{\rm en1}^2|},b_1,b_3\Big) + (r_2(x_2-1)(\phi_T^s(x_2)-\phi_T^t(x_2)) + (x_2+x_3-2)\phi_T(x_2)))a_i(t_{\rm ven}^2)E_{\rm en}(t_{\rm ven}^2,1,2)h_{\rm en}\Big(\sqrt{|\alpha_{\rm en2}^2|},\sqrt{|\beta_{\rm en2}^2|},b_1,b_3\Big)\Big\}, \tag{38}$$

(ii) $(V-A)\,(V+A)$ nonfactorizable emission diagrams with vector meson emission:

$$F_{\rm ven}^{LR}(a_i) = \frac{32}{3}\pi m_B^4 C_F r_3 \int_0^1 dx_1 dx_2 dx_3 \int_0^{1/\Lambda_{\rm QCD}} b_1 db_1 b_3 db_3 \phi_B(x_1)\Big\{(r_2((x_2-1)(\phi_T^s(x_2)-\phi_T^t(x_2))(\phi_V^s(x_3) + \phi_V^t(x_3)) - x_3(\phi_T^s(x_2)+\phi_T^t(x_2))(\phi_V^s(x_3)-\phi_V^t(x_3))) + x_3\phi_T(x_2)(\phi_V^s(x_3)-\phi_V^t(x_3)))a_i(t_{\rm ven}^1) \times E_{\rm en}(t_{\rm ven}^1,1,2)h_{\rm en}\Big(\sqrt{|\alpha_{\rm en1}^2|},\sqrt{|\beta_{\rm en1}^2|},b_1,b_3\Big) - (r_2(x_2(\phi_V^s(x_3)-\phi_V^t(x_3))(\phi_T^s(x_2)-\phi_T^t(x_2)) + x_3(\phi_V^s(x_3)+\phi_V^t(x_3))(\phi_T^s(x_2)+\phi_T^t(x_2)) - 2(\phi_V^s(x_3)\phi_T^s(x_2)+\phi_V^t(x_3)\phi_T^t(x_2))) - (x_3-1)\phi_T(x_2)(\phi_V^s(x_3)+\phi_V^t(x_3)))a_i(t_{\rm ven}^2)E_{\rm en}(t_{\rm ven}^2,1,2)h_{\rm en}\Big(\sqrt{|\alpha_{\rm en2}^2|},\sqrt{|\beta_{\rm en2}^2|},b_1,b_3\Big)\Big\}, \tag{39}$$

(iii) $(S-P)\,(S+P)$ nonfactorizable emission diagrams with vector meson emission:

$$F_{\rm ven}^{SP}(a_i) = \frac{32}{3}\pi m_B^4 C_F \int_0^1 dx_1 dx_2 dx_3 \int_0^{1/\Lambda_{\rm QCD}} b_1 db_1 b_3 db_3 \phi_B(x_1)\phi_V(x_3)\Big\{(r_2(1-x_2)(\phi_T^s(x_2)-\phi_T^t(x_2)) + \phi_T(x_2)(-x_2+x_3+1))a_i(t_{\rm ven}^1)E_{\rm en}(t_{\rm ven}^1,1,2)h_{\rm en}\Big(\sqrt{|\alpha_{\rm en1}^2|},\sqrt{|\beta_{\rm en1}^2|},b_1,b_3\Big) + (r_2(x_2-1)(\phi_T^t(x_2)+\phi_T^s(x_2)) + \phi_T(x_2)(x_3-1))a_i(t_{\rm ven}^2)E_{\rm en}(t_{\rm ven}^2,1,2)h_{\rm en}\Big(\sqrt{|\alpha_{\rm en2}^2|},\sqrt{|\beta_{\rm en2}^2|},b_1,b_3\Big)\Big\}. \tag{40}$$

(iv) $(V-A)\,(V-A)$ nonfactorizable emission diagrams with tensor meson emission:

$$F_{\rm ten}^{LL}(a_i) = \frac{32}{3}\pi m_B^4 C_F \int_0^1 dx_1 dx_2 dx_3 \int_0^{1/\Lambda_{\rm QCD}} b_1 db_1 b_2 db_2 \phi_B(x_1)\phi_T(x_2)\Big\{(x_2\phi_V(x_3) - r_3(x_3-1)(\phi_V^s(x_3) + \phi_V^t(x_3)))a_i(t_{\rm ten}^1)E_{\rm en}(t_{\rm ten}^1,1,3)h_{\rm en}\Big(\sqrt{|\alpha_{\rm en1}'^2|},\sqrt{|\beta_{\rm en1}'^2|},b_1,b_2\Big) + (r_3(x_3-1)(\phi_V^s(x_3)-\phi_V^t(x_3)) + \phi_V(x_3)(x_2+x_3-2))a_i(t_{\rm ten}^2)E_{\rm en}(t_{\rm ten}^2,1,3)h_{\rm en}\Big(\sqrt{|\alpha_{\rm en2}'^2|},\sqrt{|\beta_{\rm en2}'^2|},b_1,b_2\Big)\Big\}, \tag{41}$$

(v) $(V-A)\,(V+A)$ nonfactorizable emission diagrams with tensor meson emission:

$$F_{\rm ten}^{LR}(a_i) = \frac{32}{3}\pi m_B^4 C_F r_2 \int_0^1 dx_1 dx_2 dx_3 \int_0^{1/\Lambda_{\rm QCD}} b_1 db_1 b_2 db_2 \phi_B(x_1)\Big\{(r_3(x_2(\phi_V^s(x_3)+\phi_V^t(x_3))(\phi_T^t(x_2) - \phi_T^s(x_2)) + (1-x_3)(\phi_T^s(x_2)+\phi_T^t(x_2))(\phi_V^t(x_3)-\phi_V^s(x_3))) + x_2\phi_V(x_3)(\phi_T^s(x_2)-\phi_T^t(x_2)))a_i(t_{\rm ten}^1) \times E_{\rm en}(t_{\rm ten}^1,1,3)h_{\rm en}\Big(\sqrt{|\alpha_{\rm en1}'^2|},\sqrt{|\beta_{\rm en1}'^2|},b_1,b_2\Big) + (r_3(-x_2(\phi_V^s(x_3)+\phi_V^t(x_3))(\phi_T^s(x_2)+\phi_T^t(x_2)) + x_3(\phi_V^s(x_3)-\phi_V^t(x_3))(\phi_T^t(x_2)-\phi_T^s(x_2)) + 2(\phi_V^t(x_3)\phi_T^t(x_2)+\phi_V^s(x_3)\phi_T^s(x_2))) + (x_2-1)\phi_V(x_3)(\phi_T^s(x_2)+\phi_T^t(x_2)))a_i(t_{\rm ten}^2)E_{\rm en}(t_{\rm ten}^2,1,3)h_{\rm en}\Big(\sqrt{|\alpha_{\rm en2}'^2|},\sqrt{|\beta_{\rm en2}'^2|},b_1,b_2\Big)\Big\}, \tag{42}$$

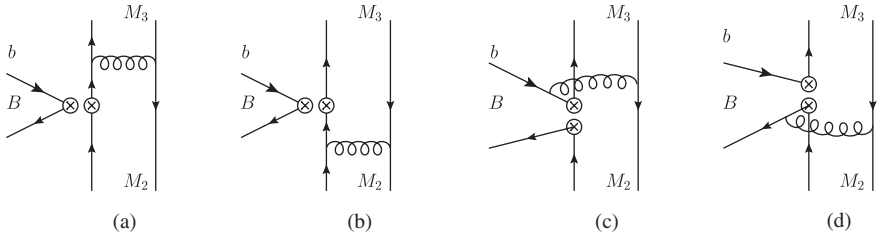

FIG. 3. The annihilation diagrams with the electroweak generated antiquark entering the tensor meson. Diagrams (a) and (b) are the factorizable contributions; diagrams (c) and (d) are nonfactorizable diagrams.

(vi) $(S-P)(S+P)$ nonfactorizable emission diagrams with tensor meson emission:

$$F_{\rm ten}^{SP}(a_i) = \frac{32}{3}\pi m_B^4 C_F \int_0^1 dx_1 dx_2 dx_3 \int_0^{1/\Lambda_{\rm QCD}} b_1 db_1 b_2 db_2 \phi_B(x_1)\phi_T(x_2)\Big\{(\phi_V(x_3)(x_2 - x_3 + 1) - r_3(x_3 - 1)(\phi_V^s(x_3) - \phi_V^t(x_3)))a_i(t_{\rm ten}^1)E_{\rm en}(t_{\rm ten}^1, 1, 3)h_{\rm en}\Big(\sqrt{|\alpha_{\rm ef1}'^2|}, \sqrt{|\beta_{\rm ef1}'^2|}, b_1, b_2\Big) + (r_3(x_3 - 1)(\phi_V^s(x_3) + \phi_V^t(x_3)) + (x_2 - 1)\phi_V(x_3))a_i(t_{\rm ten}^2)E_{\rm en}(t_{\rm ten}^2, 1, 3)h_{\rm en}\Big(\sqrt{|\alpha_{\rm en2}'^2|}, \sqrt{|\beta_{\rm en2}'^2|}, b_1, b_2\Big)\Big\}. \quad (43)$$

According to which meson has the antiquark generated from the weak vertex, the annihilation diagrams are also divided into two types, as depicted in Figs. 3 and 4. We use the first letter of the index "v" to denote the case that the quark enters the vector meson and "t" to denote that the quark enters the tensor meson. For the factorizable annihilation diagrams, which are the first two diagrams in Figs. 3 and 4, the corresponding functions are given as follows.

(i) $(V-A)(V-A)$ factorizable annihilation diagrams with the quark entering the vector meson:

$$F_{\rm vaf}^{LL}(a_i) = 8\sqrt{\frac{2}{3}}\pi m_B^4 f_B C_F \int_0^1 dx_2 dx_3 \int_0^{1/\Lambda_{\rm QCD}} b_2 db_2 b_3 db_3 \Big\{(-2r_2 r_3 \phi_V^s(x_3)(-\phi_T^s(x_2)(x_2 + 1) + \phi_T^t(x_2)(1 - x_2)) - x_2\phi_T(x_2)\phi_V(x_3))a_i(t_{\rm vaf}^1)E_a(t_{\rm vaf}^1)h_a\Big(\sqrt{|\alpha_{af1}^2|}, \sqrt{|\beta_{af1}^2|}, b_2, b_3\Big)S_t(x_2) + (-2r_2 r_3 \phi_T^s(x_2)((2 - x_3)\phi_V^s(x_3) + x_3\phi_V^t(x_3)) + (1 - x_3)\phi_T(x_2)\phi_V(x_3))a_i(t_{\rm vaf}^2)E_a(t_{\rm vaf}^2)h_a\Big(\sqrt{|\alpha_{af2}^2|}, \sqrt{|\beta_{af2}^2|}, b_3, b_2\Big)S_t(x_3)\}, \quad (44)$$

(ii) $(V-A)(V+A)$ factorizable annihilation diagrams with the quark entering the vector meson:

$$F_{\rm vaf}^{LR}(a_i) = F_{\rm vaf}^{LL}(a_i), \quad (45)$$

(iii) $(S-P)(S+P)$ factorizable annihilation diagrams with the quark entering the vector meson:

$$F_{\rm vaf}^{SP}(a_i) = 16\sqrt{\frac{2}{3}}\pi m_B^4 f_B C_F \int_0^1 dx_2 dx_3 \int_0^{1/\Lambda_{\rm QCD}} b_2 db_2 b_3 db_3 \Big\{(r_2 x_2 \phi_V(x_3)(\phi_T^t(x_2) - \phi_T^s(x_2)) + 2r_3\phi_T(x_2)\phi_V^s(x_3))a_i(t_{\rm vaf}^1)E_a(t_{\rm vaf}^1)h_a\Big(\sqrt{|\alpha_{af1}^2|}, \sqrt{|\beta_{af1}^2|}, b_2, b_3\Big)S_t(x_2) + (r_3(1 - x_3)\phi_T(x_2)(\phi_V^s(x_3) + \phi_V^t(x_3)) - 2r_2\phi_T^s(x_2)\phi_V(x_3))a_i(t_{\rm vaf}^2)E_a(t_{\rm vaf}^2)h_a\Big(\sqrt{|\alpha_{af2}^2|}, \sqrt{|\beta_{af2}^2|}, b_3, b_2\Big)S_t(x_3)\}, \quad (46)$$

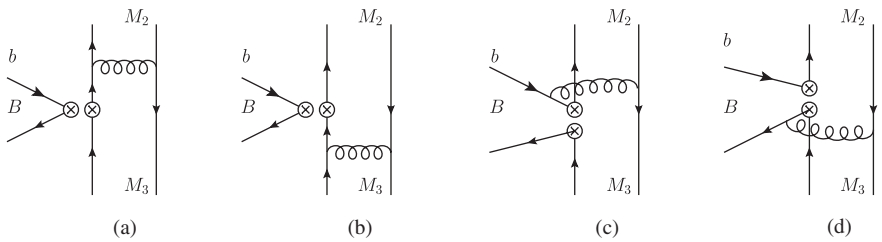

FIG. 4. The annihilation diagrams with the electroweak generated antiquark entering the vector meson. Diagrams (a) and (b) are the factorizable contributions; diagrams (c) and (d) are nonfactorizable diagrams.

(iv) $(V-A)\,(V-A)$ factorizable annihilation diagrams with the quark entering the tensor meson:

$$F_{\rm taf}^{LL}(a_i) = 8\sqrt{\frac{2}{3}}\pi m_B^4 f_B C_F \int_0^1 dx_2 dx_3 \int_0^{1/\Lambda_{\rm QCD}} b_2 db_2 b_3 db_3 \Big\{(2r_2 r_3 \phi_T^s(x_2)((x_3+1)\phi_V^s(x_3) + (x_3-1)\phi_V^t(x_3)) - x_3\phi_T(x_2)\phi_V(x_3))a_i(t_{\rm taf}^1)E_a(t_{\rm taf}^1)h_a\Big(\sqrt{|\alpha_{af1}'^2|}, \sqrt{|\beta_{af1}'^2|}, b_3, b_2\Big)S_t(x_3) + (2r_2 r_3 \phi_V^s(x_3)((x_2-2)\phi_T^s(x_2) - x_2\phi_T^t(x_2)) + (1-x_2)\phi_T(x_2)\phi_V(x_3))a_i(t_{\rm taf}^2)E_a(t_{\rm taf}^2)h_a\Big(\sqrt{|\alpha_{af2}'^2|}, \sqrt{|\beta_{af2}'^2|}, b_2, b_3\Big)S_t(x_2)\Big\}, \tag{47}$$

(v) $(V-A)\,(V+A)$ factorizable annihilation diagrams with the quark entering the tensor meson:

$$F_{\rm taf}^{LR}(a_i) = F_{\rm taf}^{LL}(a_i), \tag{48}$$

(vi) $(S-P)\,(S+P)$ factorizable annihilation diagrams with the quark entering the tensor meson:

$$F_{\rm taf}^{SP}(a_i) = 16\sqrt{\frac{2}{3}}\pi m_B^4 f_B C_F \int_0^1 dx_2 dx_3 \int_0^{1/\Lambda_{\rm QCD}} b_2 db_2 b_3 db_3 \Big\{(r_3 x_3 \phi_T(x_2)(\phi_V^t(x_3) - \phi_V^s(x_3)) + 2r_2\phi_T^s(x_2)\phi_V(x_3))a_i(t_{\rm taf}^1)E_a(t_{\rm taf}^1)h_a\Big(\sqrt{|\alpha_{\rm af1}'^2|}, \sqrt{|\beta_{\rm af1}'^2|}, b_3, b_2\Big)S_t(x_3) + (r_2\phi_V(x_3)(1-x_2)(\phi_T^s(x_2) + \phi_T^t(x_2)) - 2r_3\phi_T(x_2)\phi_V^s(x_3))a_i(t_{\rm taf}^2)E_a(t_{\rm taf}^2)h_a\Big(\sqrt{|\alpha_{\rm af2}'^2|}, \sqrt{|\beta_{\rm af2}'^2|}, b_2, b_3\Big)S_t(x_2)\Big\}. \tag{49}$$

The nonfactorizable annihilation diagrams are depicted by the last two diagrams in Figs. 3 and 4, and their corresponding functions are given in the following.

(i) $(V-A)\,(V-A)$ nonfactorizable annihilation diagrams with the quark entering the vector meson:

$$F_{\rm van}^{LL}(a_i) = \frac{32}{3}\pi m_B^4 C_F \int_0^1 dx_1 dx_2 dx_3 \int_0^{1/\Lambda_{\rm QCD}} b_1 db_1 b_3 db_3 \phi_B(x_1)\Big\{(r_2 r_3 \phi_T^s(x_2)(\phi_V^s(x_3)(x_2 - x_3 + 3) + \phi_V^t(x_3)(x_2 + x_3 - 1)) - r_2 r_3 \phi_T^t(x_2)(\phi_V^s(x_3)(x_2 + x_3 - 1) + \phi_V^t(x_3)(x_2 - x_3 - 1)) + (x_3 - 1)\phi_T(x_2)\phi_V(x_3))a_i(t_{\rm van}^1)E_{\rm an}(t_{\rm van}^1)h_{\rm an}\Big(\sqrt{|\alpha_{\rm an1}^2|}, \sqrt{|\beta_{\rm an1}^2|}, b_2, b_1\Big) + (r_2 r_3 \phi_T^s(x_2)(\phi_V^s(x_3)(-x_2 + x_3 - 1) + \phi_V^t(x_3)(x_2 + x_3 - 1)) - r_2 r_3 \phi_T^t(x_2)(\phi_V^s(x_3)(x_2 + x_3 - 1) + \phi_V^t(x_3)(-x_2 + x_3 - 1)) + x_2\phi_T(x_2)\phi_V(x_3))a_i(t_{\rm van}^2)E_{\rm an}(t_{\rm van}^2)h_{\rm an}\Big(\sqrt{|\alpha_{\rm an2}^2|}, \sqrt{|\beta_{\rm an2}^2|}, b_2, b_1\Big)\Big\}, \tag{50}$$

(ii) $(V-A)\,(V+A)$ nonfactorizable annihilation diagrams with the quark entering the vector meson:

$$F_{\rm van}^{LR}(a_i) = \frac{32}{3}\pi m_B^4 C_F \int_0^1 dx_1 dx_2 dx_3 \int_0^{1/\Lambda_{\rm QCD}} b_1 db_1 b_3 db_3 \phi_B(x_1)\Big\{(r_2\phi_V(x_3)(2-x_2)(\phi_T^s(x_2) + \phi_T^t(x_2)) + r_3(x_3+1)\phi_T(x_2)(\phi_V^s(x_3) - \phi_V^t(x_3)))a_i(t_{\rm van}^1)E_{\rm an}(t_{\rm van}^1)h_{\rm an}\Big(\sqrt{|\alpha_{\rm an1}^2|}, \sqrt{|\beta_{\rm an1}^2|}, b_2, b_1\Big) + (r_2 x_2 \phi_V(x_3)(\phi_T^s(x_2) + \phi_T^t(x_2)) + r_3(1-x_3)\phi_T(x_2)(\phi_V^s(x_3) - \phi_V^t(x_3)))a_i(t_{\rm van}^2) \times E_{\rm an}(t_{\rm van}^2)h_{\rm an}\Big(\sqrt{|\alpha_{\rm an2}^2|}, \sqrt{|\beta_{\rm an2}^2|}, b_2, b_1\Big)\Big\}, \tag{51}$$

(iii) $(S-P)\,(S+P)$ nonfactorizable annihilation diagrams with the quark entering the vector meson:

$$F_{\rm van}^{SP}(a_i)=\frac{32}{3}\pi m_B^4 C_F\int_0^1 dx_1dx_2dx_3\int_0^{1/\Lambda_{\rm QCD}} b_1db_1b_3db_3\phi_B(x_1)\Big\{(r_2r_3\phi_T^s(x_2)(\phi_V^s(x_3)(x_2-x_3+3)$$
$$-\phi_V^t(x_3)(x_2+x_3-1))-r_2r_3\phi_T^t(x_2)(\phi_V^t(x_3)(x_2-x_3-1)-\phi_V^s(x_3)(x_2+x_3-1))$$
$$-x_2\phi_T(x_2)\phi_V(x_3))a_i(t_{\rm van}^1)E_{\rm an}(t_{\rm van}^1)h_{\rm an}\Big(\sqrt{|\alpha_{\rm an1}^2|},\sqrt{|\beta_{\rm an1}^2|},b_2,b_1\Big)+(r_2r_3(-\phi_T^s(x_2)(\phi_V^s(x_3)(x_2-x_3+1)$$
$$+\phi_V^t(x_3)(x_2+x_3-1))+r_2r_3\phi_T^t(x_2)(\phi_V^t(x_3)(x_2-x_3+1)+\phi_V^s(x_3)(x_2+x_3-1))$$
$$-(x_3-1)\phi_T(x_2)\phi_V(x_3))a_i(t_{\rm van}^2)E_{\rm an}(t_{\rm van}^2)h_{\rm an}\Big(\sqrt{|\alpha_{\rm an2}^2|},\sqrt{|\beta_{\rm an2}^2|},b_2,b_1\Big)\Big\}, \tag{52}$$

(iv) $(V-A)\,(V-A)$ nonfactorizable annihilation diagrams with the quark entering the tensor meson:

$$F_{\rm tan}^{LL}(a_i)=\frac{32}{3}\pi m_B^4 C_F\int_0^1 dx_1dx_2dx_3\int_0^{1/\Lambda_{\rm QCD}} b_1db_1b_3db_3\phi_B(x_1)\Big\{(r_2r_3\phi_T^s(x_2)(\phi_V^s(x_3)(-x_2+x_3+3)$$
$$-\phi_V^t(x_3)(x_2+x_3-1))+r_2r_3\phi_T^t(x_2)(\phi_V^s(x_3)(x_2+x_3-1)-\phi_V^t(x_3)(-x_2+x_3-1))$$
$$-(1-x_2)\phi_T(x_2)\phi_V(x_3))a_i(t_{\rm van}^1)E_{\rm an}(t_{\rm tan}^1)h_{\rm an}\Big(\sqrt{|\alpha_{\rm an1}'^2|},\sqrt{|\beta_{\rm an1}'^2|},b_2,b_1\Big)$$
$$+(-r_2r_3\phi_T^s(x_2)(\phi_V^s(x_3)(-x_2+x_3+1)+\phi_V^t(x_3)(x_2+x_3-1))+r_2r_3\phi_T^t(x_2)(\phi_V^s(x_3)(x_2+x_3-1)$$
$$+\phi_V^t(x_3)(-x_2+x_3+1))+x_3\phi_T(x_2)\phi_V(x_3))a_i(t_{\rm van}^2)E_{\rm an}(t_{\rm tan}^2)h_{\rm an}\Big(\sqrt{|\alpha_{\rm an2}'^2|},\sqrt{|\beta_{\rm an2}'^2|},b_2,b_1\Big)\Big\}, \tag{53}$$

(v) $(V-A)\,(V+A)$ nonfactorizable annihilation diagrams with the quark entering the tensor meson:

$$F_{\rm tan}^{LR}(a_i)=\frac{32}{3}\pi m_B^4 C_F\int_0^1 dx_1dx_2dx_3\int_0^{1/\Lambda_{\rm QCD}} b_1db_1b_3db_3\phi_B(x_1)\Big\{-(r_2\phi_V(x_3)(x_2+1)(\phi_T^t(x_2)-\phi_T^s(x_2))$$
$$+r_3\phi_T(x_2)(x_3-2)(\phi_V^s(x_3)+\phi_V^t(x_3)))a_i(t_{\rm van}^1)E_{\rm an}(t_{\rm tan}^1)h_{\rm an}\Big(\sqrt{|\alpha_{\rm an1}'^2|},\sqrt{|\beta_{\rm an1}'^2|},b_2,b_1\Big)$$
$$+(r_3x_3\phi_T(x_2)(\phi_V^s(x_3)+\phi_V^t(x_3))-r_2(1-x_2)\phi_V(x_3)(\phi_T^t(x_2)-\phi_T^s(x_2)))a_i(t_{\rm van}^2)$$
$$\times E_{\rm an}(t_{\rm tan}^2)h_{\rm an}\Big(\sqrt{|\alpha_{\rm an2}'^2|},\sqrt{|\beta_{\rm an2}'^2|},b_2,b_1\Big)\Big\}, \tag{54}$$

(vi) $(S-P)\,(S+P)$ nonfactorizable annihilation diagrams with the quark entering the tensor meson:

$$F_{\rm tan}^{SP}(a_i)=\frac{32}{3}\pi m_B^4 C_F\int_0^1 dx_1dx_2dx_3\int_0^{1/\Lambda_{\rm QCD}} b_1db_1b_3db_3\phi_B(x_1)\Big\{(r_2r_3\phi_T^s(x_2)(\phi_V^s(x_3)(-x_2+x_3+3)$$
$$+\phi_V^t(x_3)(x_2+x_3-1))-r_2r_3\phi_T^t(x_2)(\phi_V^s(x_3)(x_2+x_3-1)+\phi_V^t(x_3)(-x_2+x_3-1))$$
$$-x_3\phi_T(x_2)\phi_V(x_3))a_i(t_{\rm van}^1)E_{\rm an}(t_{\rm tan}^1)h_{\rm an}\Big(\sqrt{|\alpha_{\rm an1}'^2|},\sqrt{|\beta_{\rm an1}'^2|},b_2,b_1\Big)$$
$$+(-r_2r_3\phi_T^s(x_2)(\phi_V^s(x_3)(-x_2+x_3+1)-\phi_V^t(x_3)(x_2+x_3-1))$$
$$+r_2r_3\phi_T^t(x_2)(\phi_V^t(x_3)(-x_2+x_3+1)-\phi_V^s(x_3)(x_2+x_3-1))$$
$$-(x_2-1)\phi_T(x_2)\phi_V(x_3))a_i(t_{\rm van}^2)E_{\rm an}(t_{\rm tan}^2)h_{\rm an}\Big(\sqrt{|\alpha_{\rm an2}'^2|},\sqrt{|\beta_{\rm an2}'^2|},b_2,b_1\Big)\Big\}. \tag{55}$$

Similar to the $B\to VV$ decays, the amplitude of $B\to VT$ can be decomposed as

$$\mathcal{A}\,(\epsilon_2,\epsilon_3)=i\mathcal{A}^N+i(\epsilon_T^*\cdot\epsilon_{\bullet T}^*)\mathcal{A}^s+(\epsilon_{\mu\nu\alpha\beta}n^\mu\bar n^\nu\epsilon_T^{*\alpha}\epsilon_{\bullet T}^{*\beta})\mathcal{A}^p, \tag{56}$$

where $\mathcal{A}^N$ contains the contribution from the longitudinal polarizations, $\mathcal{A}^s$ and $\mathcal{A}^p$ represent the transversely polarized contributions. With the amplitude functions obtained in this section, the amplitude for the decay channels can be expressed. Considering the length of the paper, we will not list all the expressions of the amplitudes, but give one of the B decay amplitude as an example:

$$\begin{aligned}\mathcal{M}(B^- \to \rho^- a_2^0) = \frac{G_F}{\sqrt{2}}\Big\{ & V_{ub}V_{ud}^*\Big[F_{\rm vef}^{LL}\Big(\frac{1}{\sqrt{2}}a_1\Big) + F_{\rm ven}^{LL}\Big(\frac{1}{\sqrt{2}}C_1\Big) + F_{\rm ten}^{LL}\Big(\frac{1}{\sqrt{2}}C_2\Big) + F_{\rm vaf}^{LL}\Big(\frac{1}{\sqrt{2}}a_1\Big) + F_{\rm taf}^{LL}\Big(-\frac{1}{\sqrt{2}}a_1\Big) \\ & + F_{\rm van}^{LL}\Big(\frac{1}{\sqrt{2}}C_1\Big) + F_{tan}^{LL}\Big(-\frac{1}{\sqrt{2}}C_1\Big)\Big] - V_{tb}V_{td}^*\Big[F_{\rm vef}^{LL}\Big(\frac{1}{\sqrt{2}}a_4 + \frac{1}{\sqrt{2}}a_{10}\Big) + F_{\rm ven}^{LL}\Big(\frac{1}{\sqrt{2}}C_3 + \frac{1}{\sqrt{2}}C_9\Big) \\ & + F_{\rm ten}^{LL}\Big(-\frac{1}{\sqrt{2}}C_3 + \frac{1}{2\sqrt{2}}C_9 + \frac{3}{2\sqrt{2}}C_{10}\Big) + F_{\rm ven}^{LR}\Big(\frac{1}{\sqrt{2}}C_5 + \frac{1}{\sqrt{2}}C_7\Big) + F_{\rm ten}^{LR}\Big(-\frac{1}{\sqrt{2}}C_5 + \frac{1}{2\sqrt{2}}C_7\Big) \\ & + F_{\rm vef}^{SP}\Big(\frac{1}{\sqrt{2}}a_6 + \frac{1}{\sqrt{2}}a_8\Big) + F_{\rm ten}^{SP}\Big(\frac{3}{2\sqrt{2}}C_8\Big) + F_{\rm vaf}^{LL}\Big(\frac{1}{\sqrt{2}}a_4 + \frac{1}{\sqrt{2}}a_{10}\Big) + F_{\rm taf}^{LL}\Big(-\frac{1}{\sqrt{2}}a_4 - \frac{1}{\sqrt{2}}a_{10}\Big) \\ & + F_{\rm van}^{LL}\Big(\frac{1}{\sqrt{2}}C_3 + \frac{1}{\sqrt{2}}C_9\Big) + F_{\rm tan}^{LL}\Big(-\frac{1}{\sqrt{2}}C_3 - \frac{1}{\sqrt{2}}C_9\Big) + F_{\rm van}^{LR}\Big(\frac{1}{\sqrt{2}}C_5 + \frac{1}{\sqrt{2}}C_7\Big) \\ & + F_{\rm tan}^{LR}\Big(-\frac{1}{\sqrt{2}}C_5 - \frac{1}{\sqrt{2}}C_7\Big) + F_{\rm vaf}^{SP}\Big(\frac{1}{\sqrt{2}}a_6 + \frac{1}{\sqrt{2}}a_8\Big) + F_{\rm taf}^{SP}\Big(-\frac{1}{\sqrt{2}}a_6 - \frac{1}{\sqrt{2}}a_8\Big)\Big]\Big\}. \end{aligned} \tag{57}$$

III. NUMERICAL RESULTS AND DISCUSSIONS

With the amplitudes calculated in Sec. II C, the decay width is given as

$$\Gamma = \frac{[(1-(r_2+r_3)^2)(1-(r_2-r_3)^2)]^{1/2}}{16\pi m_B}\sum_i |A_i|^2, \tag{58}$$

where i represents all the polarization states, and the branching ratio is obtained through $\mathcal{BR} = \Gamma\tau_B$. The key observables of the decays related in this paper are the CP averaged branching ratios, polarization fractions, as well as direct CP asymmetries ($A_{CP}^{\rm dir}$). Readers are referred to Ref. [37] for reviews on CP violation. First, we define four amplitudes as follows:

$$\begin{aligned} A_f &= \langle f|\mathcal{H}|B\rangle, \qquad \bar{A}_f = \langle f|\mathcal{H}|\bar{B}\rangle, \\ A_{\bar{f}} &= \langle \bar{f}|\mathcal{H}|B\rangle, \qquad \bar{A}_{\bar{f}} = \langle \bar{f}|\mathcal{H}|\bar{B}\rangle, \end{aligned} \tag{59}$$

where the $\bar{B}$ meson has a b quark in it and $\bar{f}$ is the CP conjugate state of f. The direct CP asymmetry $A_{CP}^{\rm dir}$ is defined by

$$A_{CP}^{\rm dir} = \frac{|\bar{A}_{\bar{f}}|^2 - |A_f|^2}{|\bar{A}_{\bar{f}}|^2 + |A_f|^2}. \tag{60}$$

Our results for CP averaged branching ratios and CP asymmetries are listed in Tables V, VI, and VII. In these tables, we also list the results of the longitudinal polarization fractions $\mathcal{R}_L$, which are defined by

$$\mathcal{R}_L = \frac{|A_0|^2}{\sum_i |A_i|^2}, \tag{61}$$

where A_0 is the amplitude of the longitudinal polarization. The first error entries of our results are from the parameters in the wave functions, the decay constant f_B and the shape parameter ω_b. The second ones are from $\Lambda_{\rm QCD}$, which varies 20% for error estimates, and from the scale t, which are listed in the Appendix.

Before we go to the numerical discussions of Tables V, VI, and VII, we note a few comments on the present experimental status. Only four channels, $B^- \to K_2^{*-}(\phi,\omega)$ and $\bar{B}^0 \to K_2^{*0}(\phi,\omega)$, are reported by *BABAR* [1,2,14], which are shown in Tables III and IV. We also collect the corresponding decays in $B \to VV$ mode [3] for

TABLE III. The pQCD results for $B \to VT$ decays which have experimental data, where the experimental data is from the *BABAR* Collaboration [1,2,14] (unit 10^{-6} for branching ratios, and % for the $\mathcal{R}_L$).

	$\mathcal{BR}$		$\mathcal{R}_L$	
Decay	This work	Experiments	This work	Experiments
$B^- \to K_2^*(1430)^-\omega$	$0.81^{+0.62+1.10}_{-0.54-0.62}$	21.5 ± 4.3	$47.0^{+0.8+0.3}_{-4.2-5.2}$	56 ± 11
$\bar{B}^0 \to \bar{K}_2^*(1430)^0\omega$	$0.93^{+0.71+1.04}_{-0.51-0.73}$	10.1 ± 2.3	$55.6^{+3.1+3.0}_{-1.5-3.2}$	45 ± 12
$B^- \to K_2^*(1430)^-\phi$	$9.1^{+3.4+2.9}_{-2.6-2.0}$	8.4 ± 2.1	$82.1^{+6.2+8.7}_{-6.6-9.2}$	80 ± 10
$\bar{B}^0 \to \bar{K}_2^*(1430)^0\phi$	$8.7^{+3.1+2.7}_{-2.5-1.9}$	7.5 ± 1.0	$82.0^{+6.5+8.1}_{-6.2-9.7}$	$90.1^{+5.9}_{-6.9}$

TABLE IV. The experimental branching ratios of $B \to K_2^*(1430)(\omega, \phi)$ decays [1,2,14] and their corresponding $B \to VV$ decays [3]. The unit is 10^{-6}.

Decays	$\mathcal{BR}$	Decays	$\mathcal{BR}$
$B^- \to K_2^*(1430)^-\omega$	21.5 ± 4.3	$B^- \to K^{*-}\omega$	$2.4 \pm 1.0 \pm 0.2$
$\bar{B}^0 \to \bar{K}_2^*(1430)^0\omega$	10.1 ± 2.3	$\bar{B}^0 \to \bar{K}^{*0}\omega$	2.0 ± 0.5
$B^- \to K_2^*(1430)^-\phi$	8.4 ± 2.1	$B^- \to K^{*-}\phi$	10.0 ± 2.0
$\bar{B}^0 \to \bar{K}_2^*(1430)^0\phi$	7.5 ± 1.0	$\bar{B}^0 \to \bar{K}^{*0}\phi$	9.8 ± 0.6

comparison. For the helicity structures of $B \to VT$ decays are very similar to the $B \to VV$ ones, a comparison between $B \to VT$ and $B \to VV$ would be very enlightening.

Comparing with the experimental data, one can see that the pQCD can give good predictions for the $B \to \phi(K_2^{*-}, \bar{K}_2^{*0})$ decays. For the $B \to \omega(K_2^{*-}, \bar{K}_2^{*0})$ decays, only the polarization fractions can be accommodated well, and large deviations exist in the branching ratios. Comparing our predictions with the experimental data, here we would like to make a few comments:

(1) $\mathcal{BR}(B \to \phi(K_2^{*-}, \bar{K}_2^{*0}))$ is very similar to $\mathcal{BR}(B \to \phi(K^{*-}, \bar{K}^{*0}))$, but a little smaller. It indicates that only small effects are brought in the branching ratios when K^* is substituted for K_2^*.

(2) However, the experimental data shows totally opposite behavior for the $B \to \omega(K_2^{*-}, \bar{K}_2^{*0}, K^{*-}, \bar{K}^{*0})$ decays, where $\mathcal{BR}(B \to \omega(K_2^{*-}, \bar{K}_2^{*0}))$ is much larger than $\mathcal{BR}(B \to \omega(K^{*-}, \bar{K}^{*0}))$. In the $B \to VV$ case, $\mathcal{BR}(B \to \phi(K^{*-}, \bar{K}^{*0}))$ is about 5 times larger than $\mathcal{BR}(B \to \omega(K^{*-}, \bar{K}^{*0}))$, while in the $B \to VT$ case $\mathcal{BR}(B \to \phi(K_2^{*-}, \bar{K}_2^{*0}))$ is even smaller than $\mathcal{BR}(B \to \omega(K^{*-}, \bar{K}^{*0}))$.

(3) The pQCD predictions for the branching ratios of the $B \to VT$ decays are very similar to but a little smaller than the experimental data of $B \to VV$. Taking the errors into consideration, the similar numerical relationship between $\mathcal{BR}(B \to \phi(K^{*-}, \bar{K}^{*0}))$ and $\mathcal{BR}(B \to \omega(K^{*-}, \bar{K}^{*0}))$ mentioned above can also be accommodated in $B \to VT$ decays. As is well known, the $B \to VT$ decay is very similar to the $B \to VV$ decay mode theoretically, therefore the branching ratios in these two decay modes are expected to have the similar behavior. Based on such prejudice, the present experimental data is a little difficult to be understood.

(4) However, only *BABAR* Collaboration reported the results for $B \to \omega(K_2^{*-}, \bar{K}_2^{*0})$ up to now, thus the experimental data need to be confirmed later. On the theoretical side, the tensor meson may bring forth a new mechanism, which needs further investigation. In Ref. [11] the authors approached those channels in a different way. They used the experimental data of those channels to extract the penguin-annihilation parameters of the QCDF and predicted the other channels. By adopting the way, the experimental data could also be accommodated. However, we note more investigations are in need to understand the underlying dynamics totally.

We collect our results for $B_{u,d} \to VT$ decays in Tables V and VI, as well as the results of branching ratios under the

TABLE V. The branching ratios ($\mathcal{BR}$ in unit of 10^{-6}), polarization fractions ($\mathcal{R}_L$ in unit of %), and direct CP violation ($A_{CP}^{\rm dir}$ in unit of %) of $B^- \to VT$ decays.

	$\mathcal{BR}$				$\mathcal{R}_L$	$A_{CP}^{\rm dir}$
	This work	QCDF [11]	ISGW2 [7]	CLF [9]	This work	This work
$B^- \to \omega K_2^{*-}$	$0.81^{+0.62+1.10}_{-0.54-0.62}$	$7.5^{+19.7}_{-7.0}$	0.112	0.06	$47.0^{+0.8+0.3}_{-4.2-5.2}$	$-4.4^{+0.4+3.7}_{-0.0-2.2}$
$B^- \to \phi K_2^{*-}$	$9.1^{+3.4+2.9}_{-2.6-2.0}$	$7.4^{+25.8}_{-5.2}$	2.180	9.24	$82.1^{+6.2+8.7}_{-6.6-9.2}$	$1.5^{+0.2+0.1}_{-0.1-0.3}$
$B^- \to \rho^- a_2^0$	$12.8^{+7.1+2.4}_{-5.1-2.4}$	$8.4^{+4.7}_{-2.9}$	7.432	19.34	$93.4^{+0.8+1.2}_{-0.9-1.5}$	$6.5^{+1.4+1.6}_{-1.6-1.5}$
$B^- \to \rho^- \bar{K}_2^{*0}$	$3.9^{+1.2+1.8}_{-0.9-1.0}$	$18.6^{+50.1}_{-17.2}$			$57.6^{+1.6+1.8}_{-0.8-1.8}$	$0.43^{+0.50+0.56}_{-0.39-0.07}$
$B^- \to \rho^0 a_2^-$	$0.67^{+0.30+0.37}_{-0.20-0.20}$	$0.82^{+2.30}_{-0.95}$	0.007	0.071	$50.8^{+5.1+9.5}_{-2.4-8.1}$	$-6.5^{+0.8+11.2}_{-0.4-7.9}$
$B^- \to \rho^0 K_2^{*-}$	$2.3^{+0.6+0.8}_{-0.6-0.5}$	$10.4^{+18.8}_{-9.2}$	0.253	0.74	$67.6^{+2.2+1.9}_{-2.9-4.0}$	$-4.8^{+1.2+1.0}_{-1.8-0.9}$
$B^- \to \omega a_2^-$	$0.41^{+0.14+0.07}_{-0.14-0.06}$	$0.38^{+1.84}_{-0.36}$	0.010	0.14	$64.5^{+0.5+2.4}_{-2.8-5.1}$	$5.91^{+2.4+4.2}_{-6.9-7.0}$
$B^- \to \phi a_2^-$	$0.01^{+0.01+0.01}_{-0.00-0.00}$	$0.0003^{+0.013}_{-0.001}$	0.004	0.019	$67.4^{+0.8+4.3}_{-0.2-0.4}$	...
$B^- \to K^{*-} a_2^0$	$3.2^{+1.4+1.1}_{-0.9-0.6}$	$2.9^{+11.7}_{-2.5}$	1.852	2.80	$59.4^{+8.1+9.9}_{-7.9-10.7}$	$-4.1^{+2.9+5.8}_{-3.7-5.2}$
$B^- \to K^{*-} K_2^{*0}$	$0.39^{+0.09+0.15}_{-0.10-0.07}$	$2.1^{+4.2}_{-1.8}$			$68.1^{+0.0+5.3}_{-2.1-2.9}$	$-3.4^{+0.9+0.9}_{-1.6-5.1}$
$B^- \to K^{*0} K_2^{*-}$	$0.19^{+0.08+0.07}_{-0.06-0.05}$	$0.56^{+1.09}_{-0.38}$	0.014	0.59	$60.7^{+8.2+6.9}_{-8.8-9.8}$	$22.1^{+7.5+1.4}_{-7.7-5.2}$
$B^- \to \bar{K}^{*0} a_2^-$	$7.6^{+3.4+2.3}_{-2.7-1.9}$	$6.1^{+23.8}_{-5.4}$	4.495	8.62	$61.8^{7.3+8.9}_{-8.1-10.7}$	$-0.82^{+0.01+0.32}_{-0.25-0.27}$
$B^- \to \rho^- f_2$	$15.6^{+8.2+1.8}_{-6.1-2.2}$	$7.7^{+4.8}_{-2.9}$	8.061		$96.9^{+0.0+0.0}_{-0.0-0.0}$	$7.2^{+0.3+1.2}_{-0.6-1.3}$
$B^- \to \rho^- f_2'$	$0.11^{+0.04+0.02}_{-0.03-0.02}$	$0.07^{+0.11}_{-0.04}$	0.103		$99.3^{+0.1+0.5}_{-0.0-0.8}$	...
$B^- \to K^{*-} f_2$	$7.3^{+2.8+2.4}_{-2.2-1.5}$	$8.3^{+17.3}_{-6.7}$	2.032		$76.3^{+4.1+1.2}_{-3.6-1.5}$	$-38.6^{+1.7+3.5}_{-0.7-2.7}$
$B^- \to K^{*-} f_2'$	$1.7^{+0.5+1.0}_{-0.3-0.5}$	$12.6^{+24.0}_{-11.1}$	0.025		$15.1^{+4.2+5.1}_{-3.6-5.6}$	$-1.6^{+0.6+0.8}_{-1.0-1.2}$

TABLE VI. The branching ratios ($\mathcal{BR}$ in unit of 10^{-6}), polarization fractions ($\mathcal{R}_L$ in unit of %), and direct CP violation ($A_{CP}^{\rm dir}$ in unit of %) of $\bar{B}_d^0 \to VT$ decays.

	$\mathcal{BR}$				$\mathcal{R}_L$	$A_{CP}^{\rm dir}$
	This work	QCDF [11]	ISGW2 [7]	CLF [9]	This work	This work
$\bar{B}_d^0 \to \omega \bar{K}_2^{*0}$	$0.93^{+0.71+1.04}_{-0.51-0.73}$	$8.1^{+21.7}_{-7.6}$	0.104	0.053	$55.6^{+3.1+3.0}_{-1.5-3.2}$	$5.4^{+1.9+3.5}_{-1.7-3.3}$
$\bar{B}_d^0 \to \phi \bar{K}_2^{*0}$	$8.7^{+3.1+2.7}_{-2.5-1.9}$	$7.7^{+26.9}_{-5.5}$	2.024	8.51	$82.0^{+6.5+8.1}_{-6.2-9.7}$	...
$\bar{B}_d^0 \to \rho^- a_2^+$	$26.7^{+13.6+3.5}_{-10.2-3.9}$	$11.3^{+5.3}_{-4.6}$	14.686	36.18	$94.8^{+0.3+0.5}_{-0.3-0.6}$	$1.3^{+0.5+1.0}_{-0.4-0.9}$
$\bar{B}_d^0 \to \rho^+ a_2^-$	$0.74^{+0.19+0.16}_{-0.20-0.13}$	$1.2^{+2.6}_{-1.0}$			$88.7^{+0.8+1.3}_{-1.6-2.6}$	$7.7^{+3.2+0.6}_{-4.3-4.4}$
$\bar{B}_d^0 \to \rho^+ K_2^{*-}$	$3.4^{+1.1+1.6}_{-0.8-0.9}$	$19.8^{+52.0}_{-18.2}$			$53.9^{+1.0+1.3}_{-0.0-1.4}$	$-2.2^{+0.7+0.8}_{-0.9-0.8}$
$\bar{B}_d^0 \to \rho^0 a_2^0$	$0.68^{+0.30+0.22}_{-0.21-0.12}$	$0.39^{+1.35}_{-0.20}$	0.003	0.03	$90.7^{+1.0+1.5}_{-0.0-0.6}$	$13.6^{+2.1+5.3}_{-0.4-3.1}$
$\bar{B}_d^0 \to \rho^0 \bar{K}_2^{*0}$	$1.7^{+0.5+0.7}_{-0.4-0.4}$	$9.5^{+33.4}_{-9.5}$	0.235	0.68	$47.0^{+0.5+2.7}_{-0.8-1.7}$	$3.3^{+1.6+1.3}_{-1.1-1.9}$
$\bar{B}_d^0 \to \omega a_2^0$	$0.37^{+0.11+0.0}_{-0.12-0.03}$	$0.25^{+1.14}_{-0.19}$	0.005	0.07	$89.5^{+0.3+1.2}_{-1.6-2.5}$	$5.7^{+8.9+11.1}_{-7.0-9.9}$
$\bar{B}_d^0 \to \phi a_2^0$	$\sim 10^{-3}$	$0.001^{+0.006}_{-0.001}$	0.002	0.009	$45.0^{+1.5+4.8}_{-1.1-3.5}$	...
$\bar{B}_d^0 \to K^{*-} a_2^+$	$6.1^{+2.8+2.1}_{-1.7-1.1}$	$6.1^{+24.3}_{-5.3}$	3.477	7.25	$59.3^{+8.3+9.1}_{-5.8-9.6}$	$-17.9^{+1.6+2.6}_{-4.4-4.9}$
$\bar{B}_d^0 \to K^{*-} K_2^{*+}$	$3.0^{+0.7+1.4}_{-0.7-0.8}$	$0.43^{+0.54}_{-0.31}$			$49.8^{+0.3+0.3}_{-1.0-0.8}$	$5.9^{+3.7+4.3}_{-1.0-0.3}$
$\bar{B}_d^0 \to K^{*+} K_2^{*-}$	$3.5^{+0.9+1.7}_{-0.8-0.9}$	$0.06^{+0.09}_{-0.03}$			$49.4^{+0.3+1.2}_{-0.6-0.4}$	$-1.2^{+0.4+1.6}_{-0.6-1.2}$
$\bar{B}_d^0 \to K^{*0} \bar{K}_2^{*0}$	$4.5^{+1.3+2.2}_{-1.1-1.2}$	$0.44^{+0.88}_{-0.30}$	0.026	0.55	$40.6^{+1.9+2.7}_{-1.5-2.1}$	$6.1^{+1.4+1.3}_{-0.9-1.9}$
$\bar{B}_d^0 \to \bar{K}^{*0} a_2^0$	$3.5^{+1.7+1.4}_{-1.2-0.8}$	$3.4^{+12.4}_{-2.8}$	2.109	4.03	$60.3^{+7.9+9.7}_{-7.7-9.9}$	$-11.1^{+0.2+2.2}_{-0.1-2.0}$
$\bar{B}_d^0 \to \bar{K}^{*0} K_2^{*0}$	$5.1^{+1.4+2.3}_{-1.2-1.5}$	$1.1^{+2.9}_{-1.0}$			$55.1^{+0.7+0.0}_{-0.2-1.9}$	$0.41^{+0.22+0.31}_{-0.19-0.93}$
$\bar{B}_d^0 \to \rho^0 f_2$	$0.41^{+0.26+0.15}_{-0.16-0.07}$	$0.42^{+1.90}_{-0.44}$	0.004	0.019	$85.3^{+1.7+3.1}_{-1.1-2.0}$	$-1.9^{+0.0+5.2}_{-2.4-9.4}$
$\bar{B}_d^0 \to \rho^0 f_2'$	$0.05^{+0.02+0.01}_{-0.01-0.01}$	$0.03^{+0.06}_{-0.02}$	5×10^{-5}		$99.3^{+0.0+0.4}_{-0.0-0.8}$	...
$\bar{B}_d^0 \to \omega f_2$	$0.56^{+0.19+0.12}_{-0.16-0.11}$	$0.69^{+0.97}_{-0.36}$	0.005		$95.5^{+0.5+0.6}_{-0.5-0.9}$	$-5.7^{+5.9+7.5}_{-8.3-7.3}$
$\bar{B}_d^0 \to \omega f_2'$	$0.04^{+0.01+0.01}_{-0.01-0.01}$	$0.03^{+0.04}_{-0.01}$	6×10^{-5}		$99.2^{+0.0+0.0}_{-0.0-0.0}$	...
$\bar{B}_d^0 \to \phi f_2$	$\sim 10^{-3}$	$0.001^{+0.007}_{-0.000}0.002$	0.002		$73.0^{+1.12+5.53}_{-0.00-0.00}$	...
$\bar{B}_d^0 \to \phi f_2'$	$0.06^{+0.03+0.02}_{-0.01-0.05}$	$0.006^{+0.034}_{-0.005}$	2×10^{-5}		$10.0^{+33.1+24.6}_{-0.0-0.3}$	$0.67^{+0.0+0.59}_{-4.98-6.03}$
$\bar{B}_d^0 \to \bar{K}^{*0} f_2$	$7.1^{+3.2+2.5}_{-2.1-1.3}$	$9.1^{+8.8}_{-7.3}$	2.314		$73.8^{+5.4+4.3}_{-3.3-1.4}$	$6.1^{+0.1+1.1}_{-0.4-1.2}$
$\bar{B}_d^0 \to \bar{K}^{*0} f_2'$	$1.8^{+0.6+1.1}_{-0.4-0.6}$	$13.5^{+25.4}_{-11.9}$	0.029		$17.4^{+6.7+6.0}_{-1.5-2.5}$	...

QCDF and from the other two models. Most results of the pQCD and the QCDF agree with each other very well. For those channels, where the pQCD and the QCDF have obviously different central values, such as $B^- \to \rho^- \bar{K}_2^{*0}$ and $\bar{B}_d^0 \to \rho^+ \bar{K}_2^{*-}$, the penguin-annihilation parameters of the QCDF contribute to the differences. The penguin-annihilation parameters are the key point of the QCDF to enhance the branching ratios of $B^- \to \omega \bar{K}_2^{*-}$ and $\bar{B}_d^0 \to \omega \bar{K}_2^{*0}$ to accommodate the experimental data. We presume those parameters are the main factors for the large differences between the central values of these channels. However, taking the errors into consideration, the two different theoretical approaches can still agree with each other. On the other hand, future experimental observation of these channels may offer an opportunity to test the dynamics of the pQCD and the QCDF.

For the channels dominated by the W-emission diagrams, especially with a vector meson emitted, such as $\bar{B}_d^0 \to a_2^+ \rho^-$, the longitudinal contribution is dominating, and the polarization fraction $\mathcal{R}_L$ is around 90%. The polarization fractions of those decays dominated by the penguin diagrams are very profound. The polarization fractions of some penguin-dominating decays of $B \to VV$ decay mode like $B \to \phi K^{*0}$ are reported to be around 50% [14], which are out of expectation of the SM. This is so-called the polarization puzzle in B physics. However, one can find that the polarization fraction of $B \to \phi K_2^{*0}$ in the $B \to VT$ behaves as the SM expectation, while the $B \to \omega K_2^{*0}$ gives about 90%. In our calculation, we find that the polarization of $B \to VT$ for these channels is near to the $B \to VV$ ones. However, after we consider $r^2 = (m_T/m_B)^2$ contributions carefully, the polarizations can be accommodated to the experimental data, although the branching fractions cannot be accommodated.

From Eq. (60) one can see that the generation of the direct CP violation requires that the amplitude A_f consists of at least two parts with different weak phases. Usually they are the tree contribution and penguin contributions in the SM. Readers are referred to Ref. [14] for the related formulas and reviews. The interference of these parts will bring the direct CP violation. The magnitude of the direct CP violation is proportional to the ratio of the penguin and tree contributions. Therefore, the direct CP violation in the SM is very small, since the penguin contribution is almost

TABLE VII. The branching ratios ($\mathcal{BR}$ in unit of 10^{-6}), polarization fractions ($\mathcal{R}_L$ in unit of %), and direct CP violation ($A_{CP}^{\rm dir}$ in unit of %) of $\bar{B}_s^0 \to VT$ decays.

	$\mathcal{BR}$	$\mathcal{R}_L$	$A_{CP}^{\rm dir}$
$\bar{B}_s^0 \to \rho^- a_2^+$	$0.35^{+0.08+0.12}_{-0.11-0.08}$	$75.6^{+0.1+2.9}_{-1.5-3.4}$	$-11.0^{+3.7+4.9}_{-2.2-2.9}$
$\bar{B}_s^0 \to \rho^- K_2^{*+}$	$17.1^{+7.7+1.2}_{-6.0-1.2}$	$93.5^{+0.2+0.5}_{-0.3-0.6}$	$4.2^{+0.7+0.8}_{-0.6-1.2}$
$\bar{B}_s^0 \to \rho^+ a_2^-$	$0.15^{+0.04+0.08}_{-0.04-0.05}$	$35.7^{+0.4+6.0}_{-1.2-3.3}$	$9.2^{+1.1+8.2}_{-1.3-7.6}$
$\bar{B}_s^0 \to \rho^0 a_2^0$	$0.03^{+0.01+0.02}_{-0.01-0.01}$	$99.1^{+0.3+0.6}_{-0.1-1.2}$	$-18.1^{+3.8+2.5}_{-1.3-5.2}$
$\bar{B}_s^0 \to \rho^0 K_2^{*0}$	$0.30^{+0.13+0.14}_{-0.10-0.08}$	$42.6^{+6.2+8.0}_{-5.9-8.5}$	$7.0^{+1.4+3.3}_{-2.0-4.7}$
$\bar{B}_s^0 \to \omega a_2^0$	$\sim 10^{-3}$	$59.8^{+12.0+16.7}_{-5.6-13.3}$	$-18.8^{+1.7+12.7}_{-5.3-3.3}$
$\bar{B}_s^0 \to \omega K_2^{*0}$	$0.13^{+0.05+0.07}_{-0.04-0.03}$	$49.6^{+2.6+6.3}_{-2.1-3.8}$	$-19.2^{+4.2+6.2}_{-4.8-4.2}$
$\bar{B}_s^0 \to \phi a_2^0$	$0.04^{+0.01+0.005}_{-0.01-0.006}$	$99.2^{+0.1+0.3}_{-0.1-0.6}$	$-1.1^{+0.1+0.4}_{-1.1-2.2}$
$\bar{B}_s^0 \to \phi K_2^{*0}$	$0.36^{+0.10+0.18}_{-0.09-0.10}$	$62.2^{+3.1+2.3}_{-0.9-0.9}$	...
$\bar{B}_s^0 \to K^{*-} K_2^{*+}$	$4.5^{+1.6+1.7}_{-1.1-0.8}$	$39.9^{+7.8+11.3}_{-4.5-8.3}$	$-12.5^{+1.2+6.0}_{-0.6-4.3}$
$\bar{B}_s^0 \to K^{*+} a_2^-$	$0.66^{+0.18+0.24}_{-0.17-0.15}$	$77.8^{+1.6+2.6}_{-0.7-3.2}$	$7.1^{+3.3+3.1}_{-3.0-3.0}$
$\bar{B}_s^0 \to K^{*+} K_2^{*-}$	$6.1^{+1.5+2.5}_{-1.6-1.6}$	$59.9^{+0.3+0.7}_{-1.4-1.9}$	$-0.9^{+0.7+0.5}_{-0.6-0.4}$
$\bar{B}_s^0 \to K^{*0} a_2^0$	$0.88^{+0.25+0.15}_{-0.23-0.13}$	$90.5^{+0.6+2.3}_{-0.6-3.1}$	$5.1^{+1.6+2.5}_{-2.6-3.5}$
$\bar{B}_s^0 \to K^{*0} \bar{K}_2^{*0}$	$8.9^{+2.6+3.7}_{-2.2-2.1}$	$62.9^{+0.4+1.4}_{-1.6-2.9}$	...
$\bar{B}_s^0 \to \bar{K}^{*0} K_2^{*0}$	$6.2^{+1.9+2.2}_{-1.7-1.5}$	$34.1^{+6.3+11.8}_{-5.2-12.2}$	$-4.2^{+0.2+0.8}_{-0.3-0.6}$
$\bar{B}_s^0 \to \rho^0 f_2$	$\sim 10^{-3}$	$69.5^{+1.8+8.1}_{-7.1-9.9}$	$-23.8^{+3.1+5.6}_{-1.6-3.8}$
$\bar{B}_s^0 \to \rho^0 f_2'$	$0.12^{+0.05+0.01}_{-0.04-0.01}$	$89.8^{+0.0+0.4}_{-0.0-0.4}$	$14.2^{+0.8+2.1}_{-0.7-1.9}$
$\bar{B}_s^0 \to \omega f_2$	$0.02^{+0.004+0.008}_{-0.003-0.009}$	$99.2^{+0.1+0.2}_{-0.3-1.0}$	$-13.9^{+2.6+2.4}_{-6.4-8.1}$
$\bar{B}_s^0 \to \omega f_2'$	$0.28^{+0.13+0.09}_{-0.10-0.06}$	$26.4^{+1.7+10.3}_{-0.4-7.4}$	$-1.3^{+0.5+1.6}_{-0.0-0.5}$
$\bar{B}_s^0 \to \phi f_2$	$2.9^{+1.0+0.7}_{-0.9-0.7}$	$98.7^{+0.1+0.6}_{-0.0-1.1}$	$0.84^{+0.07+0.19}_{-0.35-0.41}$
$\bar{B}_s^0 \to \phi f_2'$	$3.1^{+1.8+0.6}_{-1.4-0.6}$	$75.3^{+3.0+3.5}_{-3.2-1.7}$	...
$\bar{B}_s^0 \to K^{*0} f_2$	$0.51^{+0.17+0.11}_{-0.16-0.13}$	$92.2^{+1.6+2.4}_{-2.7-5.1}$	$-11.9^{+4.3+5.9}_{-2.5-2.4}$
$\bar{B}_s^0 \to K^{*0} f_2'$	$0.39^{+0.13+0.14}_{-0.09-0.08}$	$59.7^{+3.2+3.3}_{-2.2-3.1}$	...

always subdominating, which can be seen in the previous section. However, there are a few very special channels in which the penguin contributions may be comparable to the tree one, as a result, sizable direct CP violation appears. Take $B^- \to K^{*-} K_2^{*0}$ as an example. In this channel, the CKM matrix elements for the tree ($V_{ub}V_{ud}^*$) and penguin contributions ($V_{tb}V_{td}^*$) are at the same order. Although the Wilson coefficients for the tree contributions are much larger, the tree operator only appears in the annihilation diagrams, not in the emission ones. Therefore the tree contributions are suppressed, and the penguin ones become comparable, which brings to a relatively large direct CP violation for this channel.

For most of the $B \to VT$ decays, the pQCD predicts the branching ratios at the order of 10^{-6}, which would be easy for the experimental observation. We also calculate the branching ratios, polarization fractions, and the direct CP violations of $\bar{B}_s \to VT$ decays, which are collected in Table VII. Most of the $\bar{B}_s$ decays are penguin dominated, whose branching ratios are mainly at the order of 10^{-7}, therefore, whose observation requires more accumulation of experimental data. However, it would be easy for the forthcoming future flavor physics experiments. If a vector meson, generated by the tree operator whose decay constant is nonzero, is emitted in a $\bar{B}_s$ decay, then such channels have a large possibility to gain a relatively large branching ratio with the order of 10^{-6}.

IV. SUMMARY

One of the valuable topics in flavor physics is studying the hadrons in the B meson decays. In recent years, inspired by the interesting experimental data, more and more studies on the B to tensor meson decays are carried on. The pQCD approach, which has been being developed for years and predicts many B meson decays successfully, is a powerful tool in the study of two body nonleptonic B meson decays. In this paper, we investigated the $B \to VT$ decays under the frame of the pQCD. We calculated all the tree level diagrams in the approach and collected all the necessary expressions in our paper, with which we can study the 39 $B \to VT$ and 23 $B_s \to VT$ decays. The branching ratios, polarization fractions, and direct CP violations are predicted.

Four channels in $B \to VT$ are reported by the experiments: $B \to \phi(K_2^{*-}, \bar{K}_2^{*0})$ and $B \to \omega(K_2^{*-}, \bar{K}_2^{*0})$. Comparing with their similar decays in the $B \to VV$ mode, these four channels have very interesting phenomena. On the experimental side, unlike the polarization puzzle in $B \to VV$

decays, the longitudinal polarization fractions of $B \to \phi(K_2^{*-}, \bar{K}_2^{*0})$ decays are around 90%, while those of the $B \to \omega(K_2^{*-}, \bar{K}_2^{*0})$ decays are around 50%. The branching ratios of $B \to \omega(K_2^{*-}, \bar{K}_2^{*0})$ are much larger than those of $B \to \phi(K_2^{*-}, \bar{K}_2^{*0})$. This is quite different from the $B \to VV$ case, where the branching ratios of $B \to \omega(K^{*-}, \bar{K}^{*0})$ are about 5 times larger than the ones of $B \to \phi(K^{*-}, \bar{K}^{*0})$. By considering the $r^2 = (m_T/m_B)^2$ corrections, although the polarization fractions can be accommodated, the branching ratios are not predicted well. This may need further experimental confirmation and theoretical investigation.

Most of the branching ratios for B^- and $\bar{B}^0$ decays are predicted to be at the order of 10^{-6}. Most of our results agree with the the ones of the QCDF. Some channels do not agree so well by the central values, which may be caused by the different dynamics, since the QCDF introduce the penguin-annihilation parameters to accommodate the experimental data and their behavior seems different from the pQCD approach. However, taking the errors into consideration, they can still agree. For the decays which contributed by the W-emission diagram, especially when the vector meson is emitted, the polarization fraction is about 90%, which is just as the expectation of the SM. The polarization fractions for the penguin dominated decays are complicated. Some are around 90% and some are 50%, just like the cases of the four channels observed by the experiments. Fortunately, the main order of the B^- and $\bar{B}^0$ decays is 10^{-6}, which would be easy for the experimental observation.

In the $\bar{B}_s^0$ decays, the branching ratios are smaller. Such tree-dominated decays as $\bar{B}_s^0 \to \rho^- K_2^{*+}$, when a vector meson is emitted, have the mechanism to gain a relatively large branching ratio at the order of 10^{-6}. Most of the others are at the order of 10^{-7}, whose observation needs more accumulation of experimental data.

ACKNOWLEDGMENTS

The work was supported by the National Research Foundation of Korea (NRF) grant funded by Korea government of the Ministry of Education, Science and Technology (MEST) (Grant No. 2011-0017430) and (Grant No. 2011-0020333). The work of Z. T. Z. was supported by the National Science Foundation of China under Grants No. 11075168, No. 11228512, and No. 11235005.

APPENDIX: FUNCTIONS FOR HARD KERNEL, SUDAKOV FACTORS, AND SCALES

The parameters in the hard part are given as follows:

$$\begin{aligned}
&\beta_{ef1}^2 = x_1(1-x_2)m_B^2, \quad \beta_{ef2}^2 = \beta_{ef1}^2, \quad \alpha_{ef1}^2 = (1-x_2)m_B^2, \quad \alpha_{ef2}^2 = x_1 m_B^2, \quad \beta_{en1}^2 = (1-x_2)(x_1-x_3)m_B^2,\\
&\beta_{en2}^2 = (1-x_2)(x_3+x_1-1)m_B^2, \quad \alpha_{en1}^2 = (1-x_2)x_1 m_B^2, \quad \alpha_{en2}^2 = \alpha_{en1}^2, \quad \beta_{af1}^2 = -x_2(1-x_3)m_B^2,\\
&\beta_{af2}^2 = \beta_{af1}^2, \quad \alpha_{af1}^2 = -x_2 m_B^2, \quad \alpha_{af2}^2 = (x_3-1)m_B^2, \quad \beta_{an1}^2 = [1-(x_3-x_1)(1-x_2)]m_B^2,\\
&\beta_{an2}^2 = (x_3+x_1-1)x_2 m_B^2, \quad \alpha_{an1}^2 = -x_2(1-x_3)m_B^2, \quad \alpha_{an2}^2 = \alpha_{an1}^2, \quad \beta_i'^2 = \beta_i^2(x_2 \leftrightarrow x_3), \quad \alpha_i'^2 = \alpha_i^2(x_2 \leftrightarrow x_3),
\end{aligned} \tag{A1}$$

where i represents any indices.

The functions for the hard parts are given by

$$\begin{aligned}
h_e(\alpha,\beta,b_1,b_2) &= K_0(\beta b_2)[\theta(b_2-b_1)I_0(b_1\alpha)K_0(b_2\alpha) + \theta(b_1-b_2)I_0(b_2\alpha)K_0(b_1\alpha)],\\
h_{en}(\alpha,\beta,b_1,b_2) &= [\theta(b_2-b_1)I_0(b_1\alpha)K_0(b_2\alpha) + \theta(b_1-b_2)I_0(b_2\alpha)K_0(b_1\alpha)] \times \left\{ \begin{array}{c} K_0(\beta b_2) \text{ for } \beta^2 > 0 \\ \frac{i\pi}{2} H_0^{(1)}(\beta b_2) \text{ for } \beta^2 < 0 \end{array} \right\},\\
h_a(\alpha,\beta,b_1,b_2) &= \left(\frac{i\pi}{2}\right)^2 H_0^{(1)}(\beta b_2)[\theta(b_2-b_1)J_0(b_1\alpha)H_0^{(1)}(b_2\alpha) + \theta(b_1-b_2)J_0(b_2\alpha)H_0^{(1)}(b_1\alpha)],\\
h_{an}(\alpha,\beta,b_1,b_2) &= \frac{i\pi}{2}[\theta(b_2-b_1)J_0(b_1\alpha)H_0^{(1)}(b_2\alpha) + \theta(b_1-b_2)J_0(b_2\alpha)H_0^{(1)}(b_1\alpha)] \times \left\{ \begin{array}{ll} K_0(\beta b_2) & \text{for } \beta^2 > 0 \\ \frac{i\pi}{2} H_0^{(1)}(\beta b_2) & \text{for } \beta^2 < 0 \end{array} \right\},
\end{aligned} \tag{A2}$$

where the K_0, I_0, J_0, and $H_0^{(1)}$ are all Bessel functions, and $H_0^{(1)}(z) = J_0(z) + iY_0(z)$.

The scales are defined as

$$t_{v\ldots}^l = \max\left[c\sqrt{|\alpha_{\ldots l}^2|}, c\sqrt{|\beta_{\ldots l}^2|}, 1/b_k, 1/b_l\right], \qquad t_{t\ldots}^l = \max\left[c\sqrt{|\alpha_{\ldots l}'^2|}, c\sqrt{|\beta_{\ldots l}'^2|}, 1/b_k, 1/b_l\right], \tag{A3}$$

where $l = 1, 2$, the "..." represents ef, en, af, or an, and $b_{k,l}$ represent the two corresponding b coordinates in the measurement of the integration. The parameter $c = 1$, and in our error estimation, we choose $c = 0.75$ and 1.25 for a rough estimation.

The expressions for the Sudakov factors and coupling constants are given as

$$\begin{aligned} E_e(t) &= \alpha_s(t)\exp[-S_B(t) - S_V(t)], \qquad E_a(t) = \alpha_s(t)\exp[-S_T(t) - S_V(t)], \\ E_{\rm en}(t) &= \left\{\begin{array}{ll} \alpha_s(t)\exp[-S_B(t) - S_T(t) - S_V(t)|_{b_2=b_1}], & \text{if vector meson emits} \\ \alpha_s(t)\exp[-S_B(t) - S_T(t) - S_V(t)|_{b_3=b_1}], & \text{if tensor meson emits} \end{array}\right\}, \\ E_{\rm an}(t) &= \alpha_s(t)\exp[-S_B(t) - S_T(t) - S_V(t)|_{b_3=b_2}], \end{aligned} \tag{A4}$$

where

$$\begin{aligned} S_B(t) &= s\left(x_1\frac{m_B}{\sqrt{2}}, b_1\right) + \frac{5}{3}\int_{1/b_1}^{t}\frac{d\bar{\mu}}{\bar{\mu}}\gamma_q(\alpha_s(\bar{\mu})), \\ S_T(t) &= s\left(x_2\frac{m_B}{\sqrt{2}}, b_2\right) + s\left((1-x_2)\frac{m_B}{\sqrt{2}}, b_2\right) + 2\int_{1/b_2}^{t}\frac{d\bar{\mu}}{\bar{\mu}}\gamma_q(\alpha_s(\bar{\mu})), \\ S_V(t) &= s\left(x_3\frac{m_B}{\sqrt{2}}, b_3\right) + s\left((1-x_3)\frac{m_B}{\sqrt{2}}, b_3\right) + 2\int_{1/b_3}^{t}\frac{d\bar{\mu}}{\bar{\mu}}\gamma_q(\alpha_s(\bar{\mu})), \end{aligned} \tag{A5}$$

with the quark anomalous dimension $\gamma_q = -\alpha_s/\pi$. The explicit form for the function $s(Q, b)$ is

$$\begin{aligned} s(Q,b) = {} & \frac{A^{(1)}}{2\beta_1}\hat{q}\ln\left(\frac{\hat{q}}{\hat{b}}\right) - \frac{A^{(1)}}{2\beta_1}(\hat{q}-\hat{b}) + \frac{A^{(2)}}{4\beta_1^2}\left(\frac{\hat{q}}{\hat{b}} - 1\right) - \left[\frac{A^{(2)}}{4\beta_1^2} - \frac{A^{(1)}}{4\beta_1}\ln\left(\frac{e^{2\gamma_E-1}}{2}\right)\right]\ln\left(\frac{\hat{q}}{\hat{b}}\right) \\ & + \frac{A^{(1)}\beta_2}{4\beta_1^3}\hat{q}\left[\frac{\ln(2\hat{q})+1}{\hat{q}} - \frac{\ln(2\hat{b})+1}{\hat{b}}\right] + \frac{A^{(1)}\beta_2}{8\beta_1^3}[\ln^2(2\hat{q}) - \ln^2(2\hat{b})], \end{aligned} \tag{A6}$$

where the variables are defined by

$$\hat{q} \equiv \ln[Q/(\sqrt{2}\Lambda)], \qquad \hat{b} \equiv \ln[1/(b\Lambda)], \tag{A7}$$

and the coefficients $A^{(i)}$ and β_i are

$$\beta_1 = \frac{33-2n_f}{12}, \qquad \beta_2 = \frac{153-19n_f}{24}, \qquad A^{(1)} = \frac{4}{3}, \qquad A^{(2)} = \frac{67}{9} - \frac{\pi^2}{3} - \frac{10}{27}n_f + \frac{8}{3}\beta_1\ln\left(\frac{1}{2}e^{\gamma_E}\right), \tag{A8}$$

n_f is the number of the quark flavors and γ_E is the Euler constant. We will use the one-loop running coupling constant, i.e., we pick up the four terms in the first line of the expression for the function $s(Q, b)$.

[1] B. Aubert *et al.* (*BABAR* Collaboration), Phys. Rev. D **79**, 052005 (2009).
[2] B. Aubert *et al.* (*BABAR* Collaboration), Phys. Rev. Lett. **101**, 161801 (2008).
[3] B. Aubert *et al.* (*BABAR* Collaboration), Phys. Rev. D **78**, 092008 (2008).
[4] G. Lopez Castro and J. H. Munoz, Phys. Rev. D **55**, 5581 (1997).
[5] J. H. Munoz, A. A. Rojas, and G. Lopez Castro, Phys. Rev. D **59**, 077504 (1999).
[6] C. S. Kim, B. H. Lim, and S. Oh, Eur. Phys. J. C **22**, 695 (2002); **24**, 665(E) (2002).
[7] C. S. Kim, J. P. Lee, and S. Oh, Phys. Rev. D **67**, 014002 (2003).
[8] N. Sharma, R. Dhir, and R. C. Verma, Phys. Rev. D **83**, 014007 (2011).
[9] J. H. Munoz and N. Quintero, J. Phys. G **36**, 095004 (2009).
[10] A. Datta, Y. Gao, A. V. Gritsan, D. London, M. Nagashima, and A. Szynkman, Phys. Rev. D **77**, 114025 (2008).
[11] H.-Y. Cheng and K.-C. Yang, Phys. Rev. D **83**, 034001 (2011).
[12] M. Beneke, G. Buchallla, M. Neubert, and C. T. Sachrajda, Phys. Rev. Lett. **83**, 1914 (1999); Nucl. Phys. **B591**, 313 (2000); **B606**, 245 (2001).
[13] Y. Y. Keum, H.-n. Li, and A. I. Sanda, Phys. Rev. D **63**, 054008 (2001).

[14] C. Amsler *et al.* (Particle Data Group Collaboration), Phys. Lett. B **667**, 1 (2008).
[15] H.-Y. Cheng, Y. Koike, and K.-C. Yang, Phys. Rev. D **82**, 054019 (2010).
[16] W. Wang, Phys. Rev. D **83**, 014008 (2011).
[17] Z.-T. Zou, X. Yu, and C.-D. Lu, Phys. Rev. D **86**, 094015 (2012).
[18] Z.-T. Zou, Z. Rui, and C.-D. Lu, Chinese Phys. C **37**, 013103 (2013).
[19] Z.-T. Zou, X. Yu, and C.-D. Lu, Phys. Rev. D **86**, 094001 (2012).
[20] Z.-T. Zou, X. Yu, and C.-D. Lu, arXiv:1208.4252.
[21] H.-n. Li and S. Mishima, Phys. Rev. D **71**, 054025 (2005); H.-n. Li, S. Mishima, and A. I. Sanda, Phys. Rev. D **72**, 114005 (2005); H.-n. Li and S. Mishima, Phys. Rev. D **74**, 094020 (2006).
[22] G. Buchalla, A. J. Buras, and M. E. Lautenbacher, Rev. Mod. Phys. **68**, 1125 (1996).
[23] A. Ali, G. Kramer, and C. D. Lu, Phys. Rev. D **58**, 094009 (1998).
[24] C. D. Lu and M. Z. Yang, Eur. Phys. J. C **28**, 515 (2003).
[25] M. Bauer and M. Wirbel, Z. Phys. C **42**, 671 (1989).
[26] Y.-Y. Keum, H.-n. Li, and A. I. Sanda, Phys. Lett. B **504**, 6 (2001); Phys. Rev. D **63**, 054008 (2001); C.-D. Lü, K. Ukai, and M.-Z. Yang, Phys. Rev. D **63**, 074009 (2001); C.-D. Lü and M.-Z. Yang, Eur. Phys. J. C **23**, 275 (2002); R. H. Li, C. D. Lu, and H. Zou, Phys. Rev. D **78**, 014018 (2008); R. H. Li, X. X. Wang, A. I. Sanda, and C. D. Lu, Phys. Rev. D **81**, 034006 (2010).
[27] A. Ali, G. Kramer, Y. Li, C. D. Lu, Y. L. Shen, W. Wang, and Y. M. Wang, Phys. Rev. D **76**, 074018 (2007).
[28] P. Ball, G. W. Jones, and R. Zwicky, Phys. Rev. D **75**, 054004 (2007).
[29] P. Ball and R. Zwicky, Phys. Lett. B **633**, 289 (2006).
[30] P. Ball and R. Zwicky, Phys. Rev. D **71**, 014029 (2005); J. High Energy Phys. 04 (2006) 046; P. Ball and G. W. Jones, J. High Energy Phys. 03 (2007) 069.
[31] D. M. Li, H. Yu, and Q. X. Shen, J. Phys. G **27**, 807 (2001).
[32] T. M. Aliev and M. A. Shifman, Phys. Lett. **112B**, 401 (1982).
[33] T. M. Aliev and M. A. Shifman, Yad. Fiz. **36**, 891 (1982) [Sov. J. Nucl. Phys. **36**, 1532 (1982)].
[34] T. M. Aliev, K. Azizi, and V. Bashiry, J. Phys. G **37**, 025001 (2010).
[35] P. Ball and V. M. Braun, Nucl. Phys. **B543**, 201 (1999).
[36] P. Ball, V. M. Braun, Y. Koike, and K. Tanaka, Nucl. Phys. **B529**, 323 (1998).
[37] I. I. Y. Bigi and A. I. Sanda, Cambridge Monogr. Part. Phys., Nucl. Phys., Cosmol. **9**, 1 (2000); G. C. Branco, L. Lavoura, and J. P. Silva, *CP Violation* (Oxford University Press, Oxford, 1999).